Journal of the Mechanics and Physics of Solids 139 (2020) 103933

Contents lists available at ScienceDirect

Journal of the Mechanics and Physics of Solids

journal homepage: www.elsevier.com/locate/jmps

Dynamic plastic deformation and failure mechanisms of individual microcapsule and its polymeric composites

Xin Zhang[a], Pengfei Wang[b], Dawei Sun[c], Xin Li[d], Jinliang An[e], T.X. Yu[f], En-Hua Yang[a,*], Jinglei Yang[f,*]

[a] School of Civil and Environmental Engineering, Nanyang Technological University, 50 Nanyang Avenue, 639798, Singapore
[b] CAS Key Laboratory of Mechanical Behavior and Design of Materials, Department of Modern Mechanics, University of Science and Technology of China, Hefei 230026, China
[c] College of Materials Science and Engineering, Beijing University of Technology, Beijing 100124, China
[d] National Laboratory of Solid State Microstructures and Department of Materials Science and Engineering, Nanjing University, Nanjing 210093, China
[e] School of Civil Engineering, Hebei University of Engineering, Handan 056038, China
[f] Department of Mechanical and Aerospace Engineering, Hong Kong University of Science and Technology, Clear Water Bay, Kowloon, Hong Kong, China

ARTICLE INFO

Article history:
Received 11 November 2019
Revised 3 March 2020
Accepted 7 March 2020
Available online 19 March 2020

Keywords:
Fracture mechanism
Microcapsules
Polymeric composites
Impact testing
Finite elements

ABSTRACT

Functional materials are widely used by introducing functional microcapsules in the matrix. The individual microcapsule can be regarded as core-shell structure in micro-level. In this study, mechanical performance of individual microcapsule with different shell types (PUF, silica, and nickel) and corresponding microcapsule-modified polymers under quasi-static as well as dynamic compressions are studied experimentally and numerically. Results show that the strength of the nickel shell-based microcapsule is two orders higher than that of the other two microcapsules at different strain rates. More cracks and fragments are observed in microcapsule subject to dynamic loading, which indicates higher energy dissipation under impact. The inclusion of nickel shell-based microcapsule does not cause strength reduction of the resulting microcapsule-modified polymer at all strain rates, while the use of PUF and silica shell-based microcapsules lead to significant reduction of the composites strengths. Nickel shell-based microcapsule-modified polymer shows high strain rate sensitivity than the other two microcapsule-modified polymers. Furthermore, nickel shell-based microcapsule-modified polymer shows distinct failure modes when compared to the PUF and the silica shell-based microcapsule-modified polymers. While matrix cracks tend to penetrate through the weak PUF and silica shell-based microcapsules, they often propagate along the nickel shell-based microcapsule/epoxy matrix interface due to a much higher strength of the nickel shell-based microcapsule. After debonding, sliding of the fracture surfaces may lead to the final fracture of some weaker Ni microcapsules in the nickel shell-based microcapsule-modified polymer.

© 2020 Elsevier Ltd. All rights reserved.

* Corresponding authors.
E-mail addresses: EHYANG@ntu.edu.sg (E.-H. Yang), maeyang@ust.hk (J. Yang).

https://doi.org/10.1016/j.jmps.2020.103933
0022-5096/© 2020 Elsevier Ltd. All rights reserved.

1. Introduction

Microcapsules have a core-shell structure in which various functional agents in solid, liquid, or gas phases as the core material are encapsulated with either polymeric or inorganic shells by various methods (Patrick et al., 2016; Vandegaer, 2012; Xue et al., 2016). During the past decade, many advanced microencapsulation techniques have been developed and functional microcapsules have been applied widely to polymeric and cement-based composites for the preparation of intelligent materials (Li and Herbert, 2012; Yin et al., 2007). However, in most cases, incorporation of functional (*e.g.,* self-healing) microcapsules may reduce the strength of matrix material due to the low strength of microcapsules. Moreover, the microcapsule-modified composites (*e.g.*, aircraft structures) may experience impact loads (*e.g.,* hail, dropped tools during maintenance, ballistic impact) during its service life (Wu et al., 2007b; Yaghoubi and Liaw, 2013). This makes the studies of the loading rate effects on the mechanical properties of individual microcapsule as well as microcapsule-modified composites important and necessary.

At the individual microcapsules level, most researchers studied the quasi-static compressive behavior of different types of microcapsules (Keller and Sottos, 2006). Yang et al. (2008) studied the polyurethane shell microcapsule with diameter ranging from 40 to 400 μm and shell thickness ranging from 2 to 17 μm. The size of the microcapsule and shell thickness in the reported range are widely used in the multi-functional materials. It is reported that the maximum load capacity of the microcapsules is 2–50 mN. Kim et al. (2010) reported the mechanical properties of alginate-chitosan shell microcapsules with a mean diameter of 20 μm and a load capacity of 1–10 μN. Keller et al. (2006) investigated the poly (urea-formaldehyde) (PUF) shell microcapsules and reported a peak load capacity of 1–7 mN. From the published literature, in general, the capsules have a diameter of 40–400 μm with a load capacity of 1 μN to 60 mN under quasi-static compression. The relatively low strength of microcapsule may be attributed to the use of organic polymer or silica as the shell material. It is therefore necessary to develop a novel microcapsule with improved strength and robustness (Zhang et al., 2018).

Dynamic response of individual microcapsule has been rarely studied. Some researchers discussed fracture of glass spheres and elastic spherical shells (*e.g.,* ping-pong ball) under compression and impact loading conditions (Cross, 2014; Pauchard and Rica, 1998; Shipway and Hutchings, 1993). Analytical analyses were carried out to evaluate the compressive response of brittle spheres and elastic hollow spheres. The elastic hollow balls tended to buckle inwards at high speed impacts while the brittle spheres suffered a surface fracture at critical tensile stress. Different deformation phenomena and failure modes were discovered, which introduced different energy absorption mechanisms. It has been reported that the ratio of wall thickness to diameter also influences the force and failure mode of a metallic thin-walled hollow sphere under dynamic impact (Li et al., 2012). It is thus of great importance to carry out in-depth investigation on the dynamic response of microcapsules.

At the composites level, many scientists (Brown et al., 2002; Rule et al., 2007; White et al., 2001; Yuan et al., 2008) investigated the effects of size, shell thickness, and concentration of the microcapsules on physical and mechanical properties of microcapsule-modified polymers. It has been concluded that addition of microcapsules toughens the epoxy matrix and increases the energy absorption capacity. Zhang et al. (2016) report that the hollow glass microcapsule-modified polymer exhibits strong strain rate sensitivity at compression. Meanwhile, different failure modes of microcapsule-modified polymers have been observed at different strain rates. Gupta et al. (2006) conducted tensile tests on syntactic foams and observed that both tensile strength and modulus decrease with increasing volume fraction of hollow glass microcapsules. Studies showed that compressive deformation of hollow glass microsphere modified epoxy resin is bending dominated, which may make the hollow glass microcapsule modified polymer compliant and slightly weaker, but absorb more compressive energy under quasi-static loading (Swetha and Kumar, 2011). The mechanical properties of microsphere (filled with a core material) modified polymers, however, have not been investigated sufficiently. It is thus of great interest to systematically study the influence of microcapsule with a liquid core on the properties of the resulting microcapsule modified polymers at both quasi-static and dynamic loading conditions.

Finite element (FE) modelling has been applied to investigate the stress field and failure behaviour of hollow spheres filled epoxy resin. However, the unit cell method can hardly predict the failure mechanism of the hollow spheres filled epoxy resin (Marur, 2004; Nguyen and Gupta, 2010). The omission of the introduction of the gas core which results in an inner pressure in the hollow sphere during the compression, and inappropriate bonding condition between the sphere and the matrix may also make the FE analysis not very accurate (Huang et al., 2016; Yu et al., 2012). A 3D model with the inclusion of sufficient microcapsules with liquid core, well distributed microcapsules, and proper microcapsule/matrix interface properties is thus required to represent the microcapsule-modified polymer more accurately.

It is of great significance to systematically investigate the mechanical properties of both the individual microcapsule and the microcapsule-modified polymers under different loading rates. In this study, three types of microcapsules with a liquid core are fabricated through different methods. Microcapsule-modified epoxy resins with different microcapsules dosage are then fabricated. Mechanical performances and failure modes of individual microcapsules and microcapsule-modified polymers under quasi-static compression and dynamic impact are evaluated and reported.

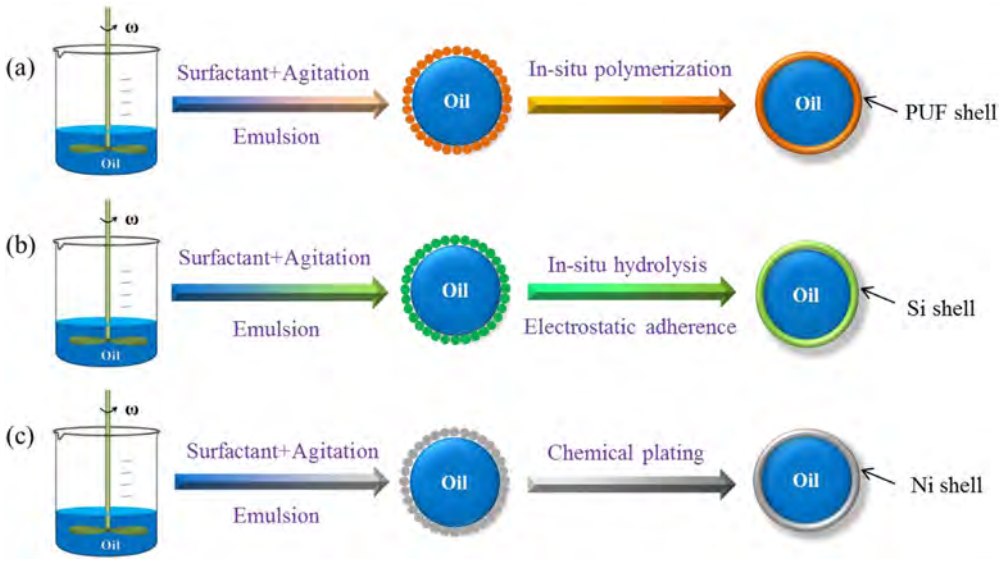

Fig. 1. Schematic illustration of synthesis process of microcapsules with (a) PUF, (b) Si, and (c) Ni shells.

2. Materials and methods

2.1. Materials and sample preparation

One conventional microcapsule with PUF shell, one novel microcapsule with silica shell, and one robust microcapsule with metal shell were fabricated. Heptadecane, a liquid wax at room temperature (~25 °C), is an oil phase material (Sarı et al., 2010). Since many other functional core materials (*e.g.*, self-healing) are also oil phase materials (Do et al., 2020; Keller and Sottos, 2006; Sun et al., 2019), heptadecane was selected as a representative core material in the current study to investigate the dynamic plastic deformation behavior and failure mechanisms of individual microcapsule and its polymeric composites. Mechanical test setups for individual microcapsule were fabricated accordingly. The synthesized microcapsules were mixed into epoxy matrix to evaluate mechanical performances of the resulting microcapsule-modified polymers. All the chemical materials used in the reaction process were purchased from Sigma Aldrich and used as received unless otherwise been clarified.

2.1.1. Synthesis of poly (urea-formaldehyde) (PUF) shell-based heptadecane microcapsules

Microcapsules were prepared through in-situ polymerization in an oil-in-water emulsion, as shown in Fig. 1a. Some amount of aqueous solution of ethylene maleic anhydride (EMA) copolymer in a beaker was placed in a temperature-controlled water bath. The solution was stirred by the mechanical stirrer. Some amount of urea, ammonium chloride and resorcinol were dissolved in the solution. Heptadecane was added into the prepared solution to form an emulsion at 55°C. After 4 h reaction, the suspension with microcapsules was separated under vacuum environment. The separated PUF microcapsules were rinsed and dried for 24 h before testing.

2.1.2. Synthesis of silica shell-based heptadecane microcapsules

The aqueous solution of Arabic gum was diluted with deionized water and the solution was kept in a beaker with a mechanical stirrer (Caframo, Model: BDC6015). Heptadecane and Hexamethylene diisocyanate (HDI) were then added into the solution to generate emulsion at 50°C. After that, Polyethyienimine (PEI, Mw~1300) solution was added into the emulsion system and agitated for 2 h. The precursor microcapsules were collected, rinsed, and re-dispersed in deionized water. Meanwhile, hydrolysis of Trimethoxymethylsilane (MTTS) was carried out in hydrochloric acid solution (HCl, 0.1 N) for 1 h. The hydrolyzed MTTS was mixed in the system for 24 h. Finally, the synthesized silica shell-based microcapsules were rinsed and collected after 24 h air-drying for further study. The synthesis process can be found in Fig. 1b.

2.1.3. Synthesis of nickel-P shell-based heptadecane microcapsules

Nickel shell-based microcapsules with liquid core were fabricated successfully through electroless plating approach, as illustrated in Fig. 1c. The heptadecane was added into surfactant solution with mechanical agitation to generate micro-droplets of heptadecane. After that, the emulsified micro-droplets solution was mixed with palladium chloride solution with mechanical agitation. Because of the surface tension, the obtained palladium particles adhered to the surface of the micro-droplets as the catalyst. Then the nickel sulfate was prepared in solution to react with the mixed micro-droplets solution.

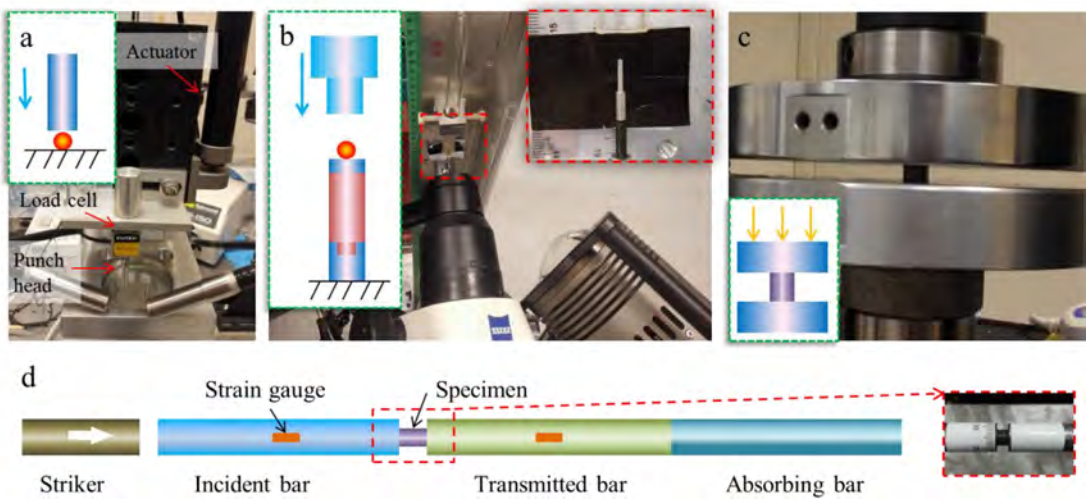

Fig. 2. (a) Quasi-static compression setup and (b) dynamic impact setup for testing individual microcapsules, and (c) quasi-static compression machine and (d) SHPB for testing microcapsule-modified epoxy resin.

The nickel alloy shell was generated at the surface of the micro-droplets during the chemical plating process. Lastly, the synthesized nickel shell-based microcapsules were washed with deionized water (DI) water and dried for 24 h for further study.

2.1.4. Fabrication of microcapsule-modified polymers

Epoxy resin and hardener (Epolam 5015/5015) purchased from Axson Technologies were mixed together with a ratio of 100 to 30, as suggested by the manufacturer Since the microcapsules are synthesized chemically and can be used as the fillers of a multi-functional composite, it will be more convenient and rational to compare the mechanical properties of the polymers with microcapsules of the same weight fraction. As a result, the synthesized microcapsules were mixed into the resin (0, 5, 10 wt.%) with a mechanical stirrer until the viscosity of the resin is relatively high, which prevents sinking of Ni microcapsules and floating of Si and PUF shell microcapsules. The suspension was degassed by using a vacuum oven (MRC, Model: 1410-DIG) which connected to a vacuum pump (Vacuubrand, Model: RZ-2.5). The suspension was cast into cylindrical silicone gel mold with release agent and cured for 24 h under room temperature. The specimens in the silicone gel mold were then cured in an oven at 60 °C for 16 h. The hardened cylindrical specimen has a diameter of 7 mm and a height of 25 mm. The middle portion of the cylinder was sliced into two specimens with a height of 5 mm by using a diamond saw (Yasuda Plastic Sample Cutting Machine). This is to ensure relatively constant weight fraction of microcapsule in the testing specimens. End surfaces of specimens were polished before further tests.

2.2. Test and analysis methods

2.2.1. Quasi-static compression on individual microcapsule

The quasi-static compression setup consists of a load cell to measure the compressive load Fig. 2a). The punch head is connected to an actuator which drives the head in a constant velocity. Three test speeds at 1 μm/s, 10 μm/s, and 100 μm/s were applied. A CCD camera with a stereo microscope (Zeiss, Stemi 2000-C) was used to take images during compression tests. The stress distributes on the core-shell structure during loading is not a uniform value (Zhang et al., 2018). In order to identify the mechanical behavior of the microcapsule, nominal stress is introduced to represent its overall mechanical property in engineering. In this study, the microcapsules are regarded as integral structures in the polymer matrix which can transfer the load and change the crack propagation and failure mode in the matrix during loading. As a result, the nominal stress (σ_n) (Pejchal et al., 2017) of the microcapsule can be expressed as Eq. (1). The nominal strain (ε_n) and loading rate ($\dot{\varepsilon}_n$) experienced by the microcapsule can be estimated using Eqs. (2) and ((3), respectively.

$$\sigma_n = \frac{P}{A} = \frac{4 \cdot P}{\pi \cdot d^2} \tag{1}$$

$$\varepsilon_n = \frac{S_{Head}}{d} \tag{2}$$

$$\dot{\varepsilon}_n = \frac{V_{Head}}{d} \tag{3}$$

where P is the load during the test, A is the cross-sectional area at the equator of the microcapsule, d is the diameter of the microcapsule, S_{Head} represents the displacement of the punch head, and V_{Head} represents the velocity of the punch head.

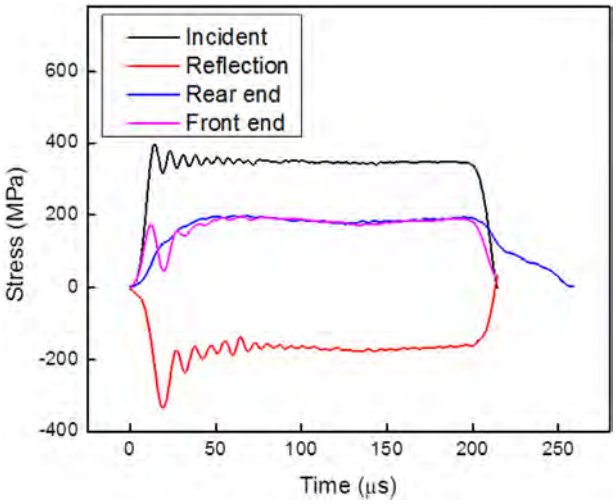

Fig. 3. Stress wave propagation during dynamic compression test.

The nominal strength is the nominal stress at the peak load while integrated failure strain is the nominal strain at the peak load. At least 10 samples were tested for each loading speed and the average value and standard deviation were reported.

2.2.2. Impact test on individual microcapsule

The impact test setup Fig. 2b) consists of an impactor which drops freely in a transparent slide guide, a high sensitive quartz-piezoelectric force sensor (Kistler 9217A) with charge amplifier (Type 5015A1000) which records the precise load during the impact, and a high speed camera (Fastcam SA4, Photron) with a stereo microscope recording at 10^5 frames per second to capture the deformation and failure mode during the impact. Two impact velocities at 0.3 m/s and 2.2 m/s were applied by adjusting the drop height of the impactor. According to the conservation of momentum, the velocity of the impactor can be assumed as a constant value since the load during the impact is very low. This phenomenon was also confirmed by the high speed camera as there was no obvious velocity change of the impactor during the impact. The nominal strain, nominal stress, and loading rate can be estimated using the same Eqs. (1)–(3). At least 8 samples were tested for each loading speed and the average value and standard deviation were reported.

2.2.3. Low strain rate compression on microcapsule-modified polymers

Instron 5569 Universal Testing Machine (UTM) was used to conduct the low strain rate compression at 0.0067 s^{-1} and 0.2 s^{-1} (Fig. 2c). Grease was applied on the two contact surfaces to reduce friction between sample and fixture. Stress-strain curve of tested specimen can be generated from the load and displacement captured from the UTM. At least 4 samples were tested for each strain rate.

2.2.4. High strain rate compression on microcapsule-modified polymers

Split-Hopkinson pressure bar (SHPB) (Guo et al., 2019) was used to conduct the high strain rate compression (Fig. 2d). Aluminum bars were used to amplify the strain signal. 50 cm striker bar was adopted to generate longer compression stress wave. Two gas gun pressures at 40 psi and 100 psi were used to achieve high strain rate loading of 1100 s^{-1} and 3200 s^{-1}, respectively. The stress applied to the front end of the specimen can be calculated through the incident and reflection stress waves. The stress applied to the rear end of the specimen can be obtained from the transmitted wave. As shown in Fig. 3, force equilibrium during high strain rate loading is largely achieved.

2.2.5. Sample characterization

Optical microscope (OM, Olympus, SZX7) and field emission scanning electron microscope (FESEM, Jeol, Model: JSM-7600F) were used to identify the fracture modes and microstructures of individual microcapsules and microcapsule-modified polymers. A thermogravimetric analysis instrument (TGA, Hi-Res Modulated TGA 2950) with a nitrogen atmosphere was adopted to investigate the thermal properties of synthesized microcapsules.

3. Theoretical model and FE model

3.1. Deformation of individual microcapsule

The mechanical property of the microcapsule is determined by both the shell and the core properties. The deformation of the microcapsule can be divided into three stages. During the first stage, when the deflection of the microcapsule is very

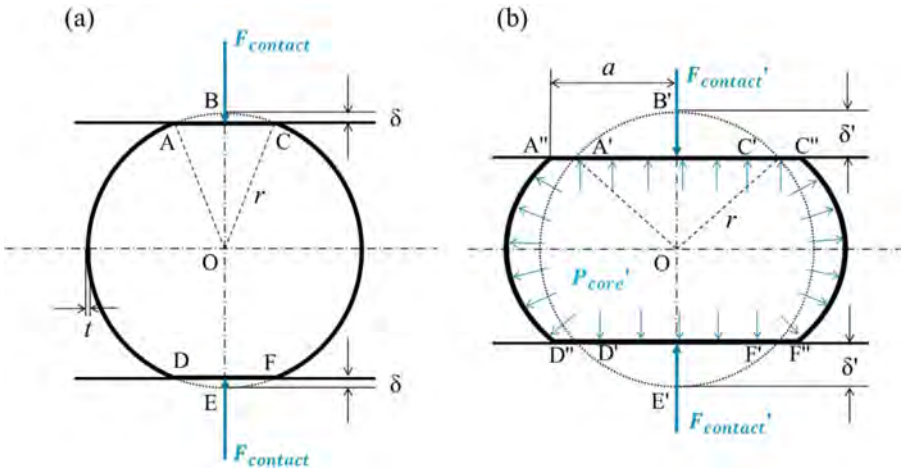

Fig. 4. Schematic illustration of (a) stage one and (b) stage two deformation of microcapsule.

small, it can be assumed that the deformation of the microcapsule is locally constrained around the two contact areas. As shown in Fig. 4a, the ABC and DEF portions of the microcapsule are flattened by the rigid punch head and the support platform. The volume change of the liquid core can be neglected. As a result, the contact force between the punch head and the microcapsule is mainly supported by the shell structure of the microcapsule, which can be calculated as follows (Bao and Yu, 2015; Reissner, 1949),

$$F_{contact} = \frac{8E_b}{rc}\delta = \frac{4E_b}{rc}D_f \tag{4}$$

$$E_b = E_{shell}tc^2 \tag{5}$$

$$c = \frac{t}{\sqrt{12\left(1-\nu^2\right)}} \tag{6}$$

where E_b is the bending stiffness of the shell structure, D_f is the deflection of the microcapsule which is two times the value of δ, E_{shell} is the elastic modulus of the shell material, t is the shell thickness, c is the reduced thickness of the shell, and ν is the Poisson's ratio.

During the second stage (as shown in Fig. 4b), with the increase of the deflection of the microcapsule, the inner pressure provided by the liquid core may increase rapidly which also improves the strength of the microcapsule. The contact force at this stage can be expressed as follows,

$$\mathrm{F}_{core} = P'_{core}\cdot S_{A''C''} = K\frac{V_0 - V'}{V_0}\pi a^2 \tag{7}$$

$$F'_{contact} = F_{contact} + F_{core} = \frac{4E_b}{rc}D_f + \pi K a^2\frac{V_0 - V'}{V_0} \tag{8}$$

where P'_{core} is the inner pressure of the liquid core, $S_{A''C''}$ is the contact area of the punch head and the microcapsule during the compression, K is the bulk modulus of heptadecane, V_0 and $V'$are the initial volume and deformed volume of the liquid core, respectively.

At the third stage, with the increase of contact force and inner pressure of the liquid core, the stress may concentrate at both the top and the bottom area of the microcapsule which may lead to failures at the two areas and generate crack at the meridional direction.

3.2. Debonding of microcapsule in matrix

The microcapsule may debond from the polymeric matrix during the compression. The energy required for a single microcapsule to fully debond from the matrix can be expressed as,

$$\mathrm{w} = G_a A = 4\pi r^2 G_a \tag{9}$$

where G_a is the fracture energy of bond (between microcapsule and matrix) per unit area, A is the surface area of the microcapsule, r is the radius of the microcapsule. It can be found that microcapsules with larger diameter require more energy for debonding. However, different stress level may be required to initiate the debonding. According to analytical

Table 1
Physical and mechanical properties of materials used in the FE simulation.

Material	Density (g/cm^3)	Elastic modulus (GPa)	Poisson ratio	Bulk modulus (GPa)	Viscosity (Pa•s)	Adhesive strength (MPa)
Epoxy	1.10	1.93	0.35	\	\	\
PUF	1.55	3.70	0.30	\	\	13.5
Nickel	7.75	98.1	0.31	\	\	13.1
Heptadecane	0.78	\	\	1.37	0.026	\

solution from Gent (1980), the minimum strain energy density (U_{min}) of a composite can be calculated as follows,

$$U_{min} = \frac{4\pi G_a}{3kr\sin 2\theta} \tag{10}$$

where θ is the polar angle and k is a constant. Since the applied stress (σ) and strain energy density can be expressed as,

$$\mathrm{U} = \frac{\sigma^2}{2E} \tag{11}$$

where E is the Young's modulus of the composite, the predicted critical stress (σ_p) for debonding of a microcapsule from matrix can be obtained through the following equation,

$$\sigma_p = \sqrt{\frac{8\pi G_a E}{3kr\sin 2\theta}} \tag{12}$$

Accordingly, microcapsules with smaller diameter require higher stress to initiate debonding.

3.3. FE modeling of microcapsule-modified polymer

Hexagonal unit structure was employed to investigate the stiffness of the microcapsule-modified polymer with capsule fraction of 0, 5, and 10% by an in-house program. Periodic boundary condition was applied on the boundary of the unit cell to achieve static loading condition by using ABAQUS (Zhang et al., 2016). The basic mechanical parameters used in the FE simulation can be found in Table 1 (Prak et al., 2017; Zhang et al., 2010).

In order to investigate the failure mechanism of microcapsule-modified polymer, a cubic 3D model with a volume of 2 mm × 2 mm × 2 mm was established. The cubic representative volume element has around 60–100 microcapsules, which adequately represents the bulk microcapsule-modified polymer composite. Fig. 5 depicts the procedure to generate microcapsules with diameters follow normal distribution, which are randomly distributed in the polymer matrix. The overlapping between microcapsules and between microcapsule and the wall of the 3D cubic model can be avoided by the following control equations in the program. A threshold distance has been set to guarantee the quality of the mesh element,

$$\sqrt{\sum_{k=1}^{3}\left(x_i^k - x_j^k\right)^2} \geq r_i + r_j + \Delta d \tag{13}$$

$$\left|x_i^m - r_i\right| \geq \Delta d \quad m = 1, 2, 3 \tag{14}$$

$$\left|x_i^m + r_i - L\right| \geq \Delta d \quad m = 1, 2, 3 \tag{15}$$

where x, r, Δd, and L are the coordinate vector of the microcapsule center, the radius of the microcapsule, threshold distance, and the length of the 3D model, respectively. Δd is not only a threshold distance to avoid the intersections among microcapsules and guarantee to restrict the microcapsules inside the matrix, but also a distance to avoid too tiny mesh in the mesh generation of the model which may generate inaccurate simulation result and dramatic longer simulation time. A Python program with control equations was employed to generate the matrix, microcapsule including shell and core structure, and cohesive layer between the matrix and the microcapsules (Fig. 6a and c). The cohesive layer was used to simulate the adhesive property between the microcapsules and the epoxy resin. The cohesive element is governed by the traction-separation law (Yu et al., 2012), which can be expressed in an elastic constitutive matrix as follows,

$$\mathrm{t} = \begin{Bmatrix} t_n \\ t_s \\ t_t \end{Bmatrix} = \begin{bmatrix} K_{nn} & K_{ns} & K_{nt} \\ K_{ns} & K_{ss} & K_{st} \\ K_{nt} & K_{st} & K_{tt} \end{bmatrix} \begin{Bmatrix} \delta_n \\ \delta_s \\ \delta_t \end{Bmatrix} = K\delta \tag{16}$$

The traction stress vector t consists of three factors: t_n, t_s, and t_t, which stand for the normal traction, traction in first shear, and traction in second shear, respectively. The damage evolution of the cohesive element may initiate when the

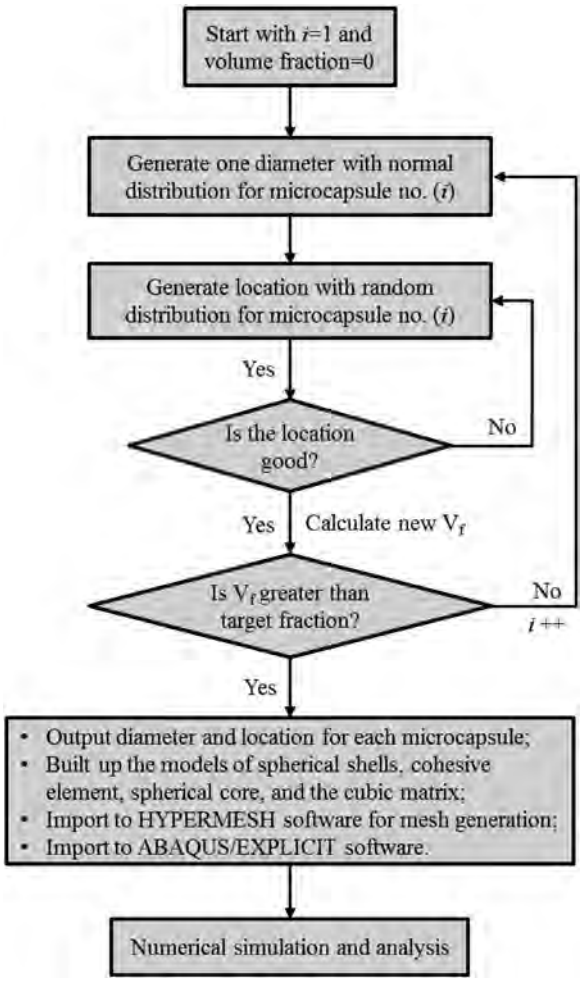

Fig. 5. Flowchart to generate the 3D FE model.

following criterion is satisfied.

$$\left(\frac{t_n}{t_{n0}}\right)^2 + \left(\frac{t_s}{t_{s0}}\right)^2 + \left(\frac{t_t}{t_{t0}}\right)^2 = 1 \tag{17}$$

where t_{n0}, t_{s0}, and t_{t0} represent the initial strength of the interface between the microcapsule and the epoxy resin.

The established 3D model was imported to HYPERMESH for mesh generation and then imported to ABAQUS/Explicit for FE analysis and post-treatment. Tetrahedral and hexahedral mesh for solid parts and quadrilateral mesh for shell parts were generated accordingly, as shown in Fig. 6b. The "us-up" model was employed to simulate the hydro pressure during compression. All the dimensions and weight fractions of microcapsules were obtained from experimental results. The basic mechanical parameters of shell materials and their adhesive properties were acquired from literature (Dilsiz and Wightman, 2000; Li et al., 2016; Ni et al., 2012; Yuan et al., 2015; Zhang et al., 2018). Other mechanical properties of materials were obtained from the experiments. In the current study, polymers modified with 5 wt.% PUF (or Ni) microcapsules were studied. The applied strain rate in the FE simulation was 3300 s^{-1}, which was similar to the testing rate in the high strain rate compression in the current study.

The compression of individual microcapsule was also investigated through FE analysis by using ABAQUS. Shell structure with shell mesh element and core structure with solid mesh element were combined and compressed between two rigid plates. The material properties and other mechanical parameters used in the FE analysis were the same as the analysis of microcapsule-modified polymer. High performance computing (HPC) is applied to carry out the finite element simulation of the compression of both the individual microcapsule and microcapsules-modified polymers.

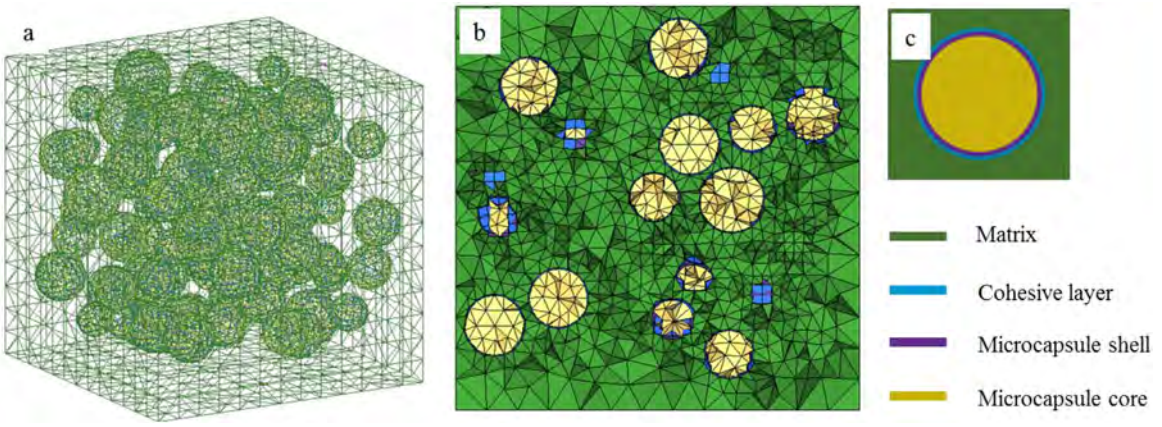

Fig. 6. (a) Meshed 3D FE model, (b) cross section of the meshed 3D FE model, and (c) detailed structure of an individual microcapsule.

4. Results and analysis

4.1. Characterization of fabricated microcapsules

The diameter of the microcapsule can be controlled by the agitation rate during the emulsion process (Yang et al., 2008). The shell thickness of the microcapsule can be controlled by adjusting the agitation rate and reaction duration during the emulsion and shell formation process (O'Sullivan et al., 2009; Wu et al., 2014). Fig. 7 shows the morphology of the three types of microcapsules. As can be seen, all microcapsules are in spherical shape (Figs. 7a1, 4b1, and 4c1). Ni microcapsule has smooth surface (Fig. 7a2) while Si microcapsule has rough surface morphology due to different synthesis processes (Fig. 7c2). The structure of the microcapsule can be defined as a typical core-shell structure with spherical heptadecane core and uniform shell. The thickness for PUF, silica, and nickel shell are approximately 4.5 μm, 4.7 μm, and 6.7 μm, respectively, which are measured from the SEM images (Fig. 7a3, b3, and c3).

The diameters of the microcapsules were measured by using the optical microscope. The size distribution of the three types of microcapsules can be found in Fig. 8a. As can be seen, the three types of capsules have similar sizes and the average diameters of PUF microcapsules, Si microcapsules, and Ni microcapsules are 218 μm, 213 μm, and 234 μm, respectively. Microcapsules with diameter from 210 μm to 290 μm were selected by the optical microscope for the tests on individual microcapsule.

Fig. 8b shows the TGA curves for the three types of microcapsules. The maximum temperature was set to 350 °C with a heating rate of 10 °C/min. As can be seen, the wax core material decomposes after 250 °C for both the PUF microcapsule and the Si microcapsule. However, the Ni shell protects the core material and delays the decomposition of wax core as the rate of weight loss in the Ni microcapsule is much lower than that in the other two microcapsules. From the TGA curve, weight fraction of the core material for the PUF microcapsule, the Si microcapsule, and the Ni microcapsule are estimated to be 88.95%, 88.02%, and 30.01%, respectively.

4.2. Mechanical properties of individual microcapsules

4.2.1. Strength

The mechanical properties of individual microcapsules were studied by means of quasi-static compression and dynamic impact. As can be seen from Fig. 9, the nominal strength for the Ni microcapsule is two orders higher than that of the Si microcapsule and the PUF microcapsule. The nominal strength of the Si microcapsule is slightly higher than that of the PUF microcapsule. The nominal strength increases with increasing strain rate, especially at high strain rates, for all three types of microcapsules. It is worth noting that the measured strength of individual microcapsule possesses noticeable variability perhaps due to the variation of shell thickness and imperfection and defects in the shell during synthesis.

The nominal strength of traditional microcapsule (PUF shell) and novel metal microcapsule (Ni shell) are studied by FE analysis (Fig. 9). As can be seen, simulation results for both the PUF and the Ni microcapsules are quite close to the experimental results, which prove the validity of the FE model and the rationality of the parameters adopted in the simulation. Furthermore, the nominal strength of microcapsule at medium loading rate (1–100 s^{-1}) can be acquired numerically which is often difficult to obtain experimentally. This provides great practical significance for engineers to investigate the mechanical properties of core-shell microcapsules.

The shell thickness of the microcapsule may affect the mechanical property of the microcapsule. Since the Ni microcapsule is much more robust than the PUF and Si microcapsules, the nominal strengths of individual Ni microcapsule with different shell thickness under two rigid plates compression are compared with the compressive strength of the epoxy resin

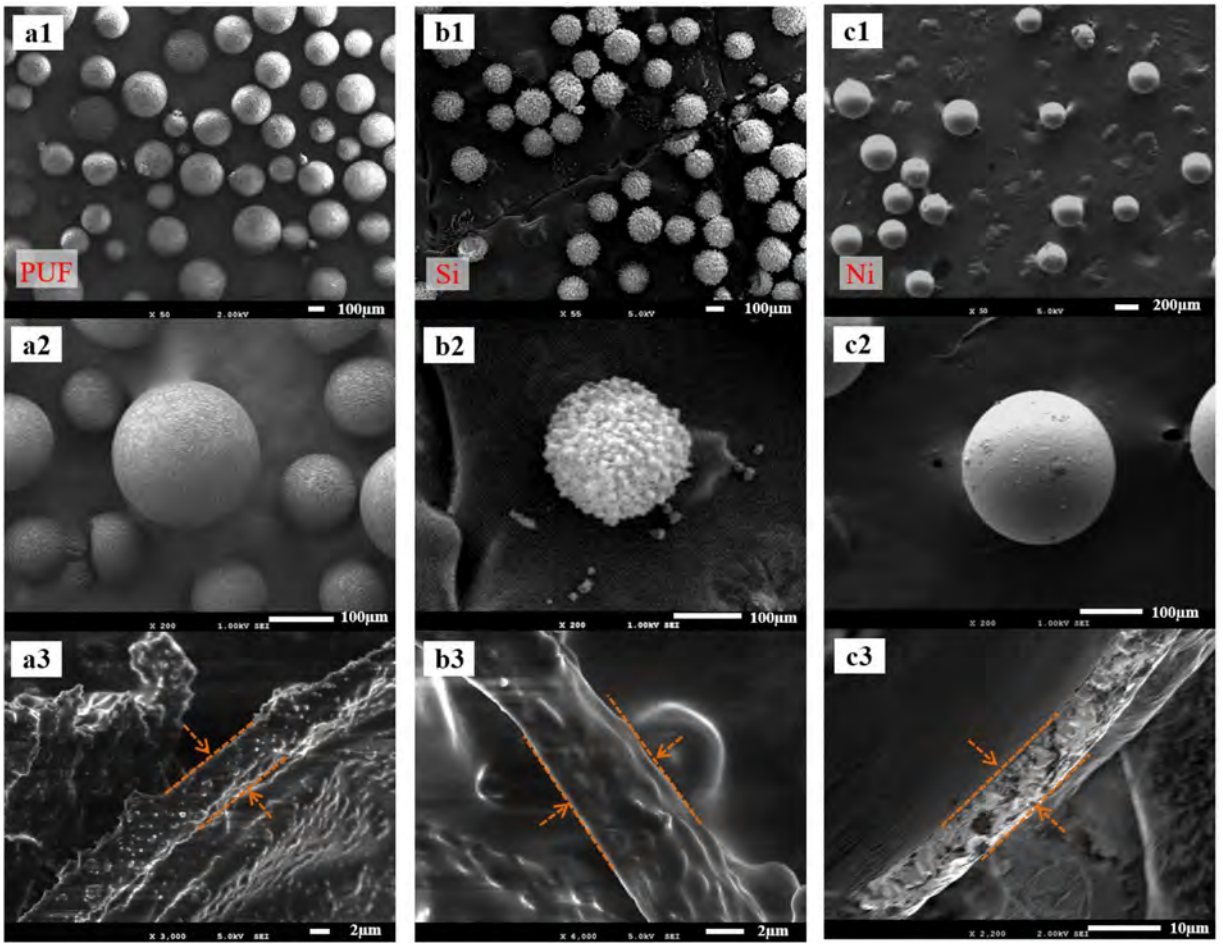

Fig. 7. (a1–a2) PUF microcapsule and (a3) its shell structure, (b1-b2) Si microcapsule and (b3) its shell structure, and (c1-c2) Ni microcapsule and (c3) its shell structure.

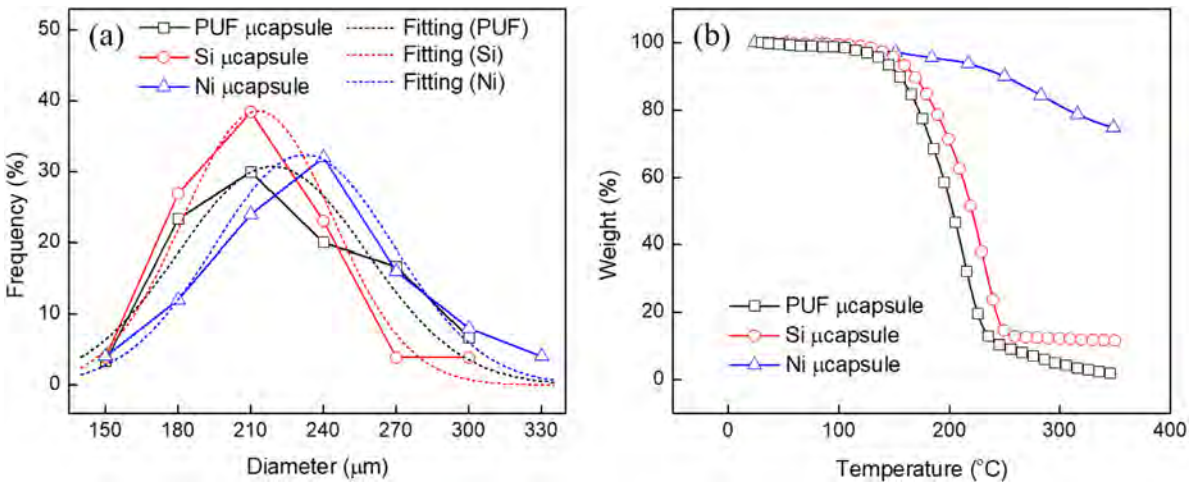

Fig. 8. (a) Size distributions and (b) TGA curves of PUF, Si, and Ni microcapsules.

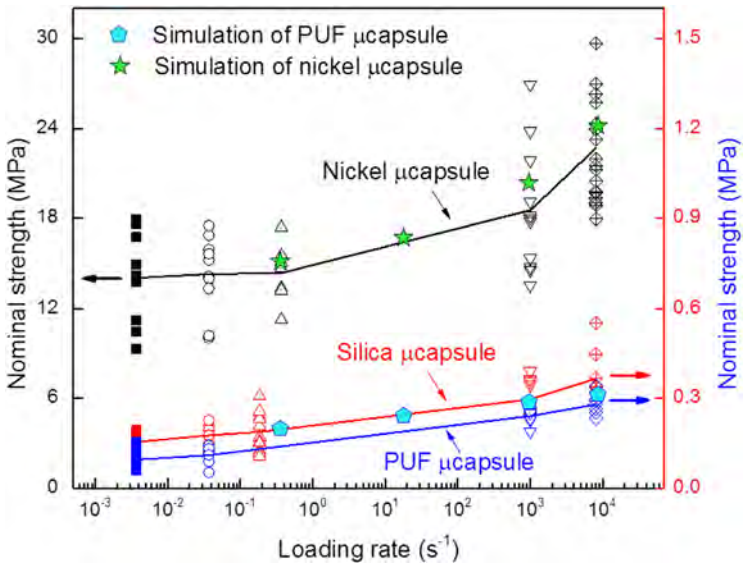

Fig. 9. Nominal strength of microcapsules as a function of strain rate from experiment results and FE analysis.

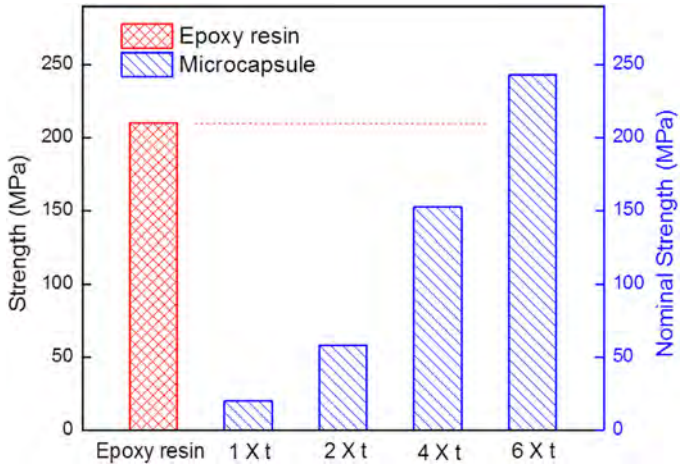

Fig. 10. Strength of pure epoxy resin and nominal strength of individual Ni microcapsule with different shell thicknesses.

at a loading rate of about 3300 s^{-1} (Fig. 10). As can be seen, the nominal strength of the Ni microcapsule increases with increasing shell thickness. It is worth noting that when the shell thickness increases to six times that of the original shell thickness, the nominal strength of the microcapsule exceeds the strength of epoxy resin.

4.2.2. Weibull distribution and strain rate sensitivity

To characterize this variability of strength in different types of microcapsules, the Weibull strength distribution model (Vu et al., 2018; Wang et al., 2018, 2016) that takes loading rate into consideration was adopted to investigate the cumulative probability of failure of single microcapsule as follows,

$$P_f(\sigma) = 1 - exp\left[-\dot{\varepsilon}^k\left[\frac{\sigma}{\sigma_{\dot{\varepsilon}}}\right]^m\right] \tag{18}$$

where $\sigma_{\dot{\varepsilon}}$ is the strain rate dependent scale parameter, k is the strain rate dependent parameter which is a constant, and m is the Weibull modulus. Eq. (19) describes the average strength of individual microcapsule as follow,

$$\bar{\sigma} = D\dot{\varepsilon}^{-\frac{k}{m}} \tag{19}$$

where $D = \sigma_{\dot{\varepsilon}}\Gamma(1+\frac{1}{m})$ is a constant and $\Gamma(1+\frac{1}{m})$ is a Gamma function.

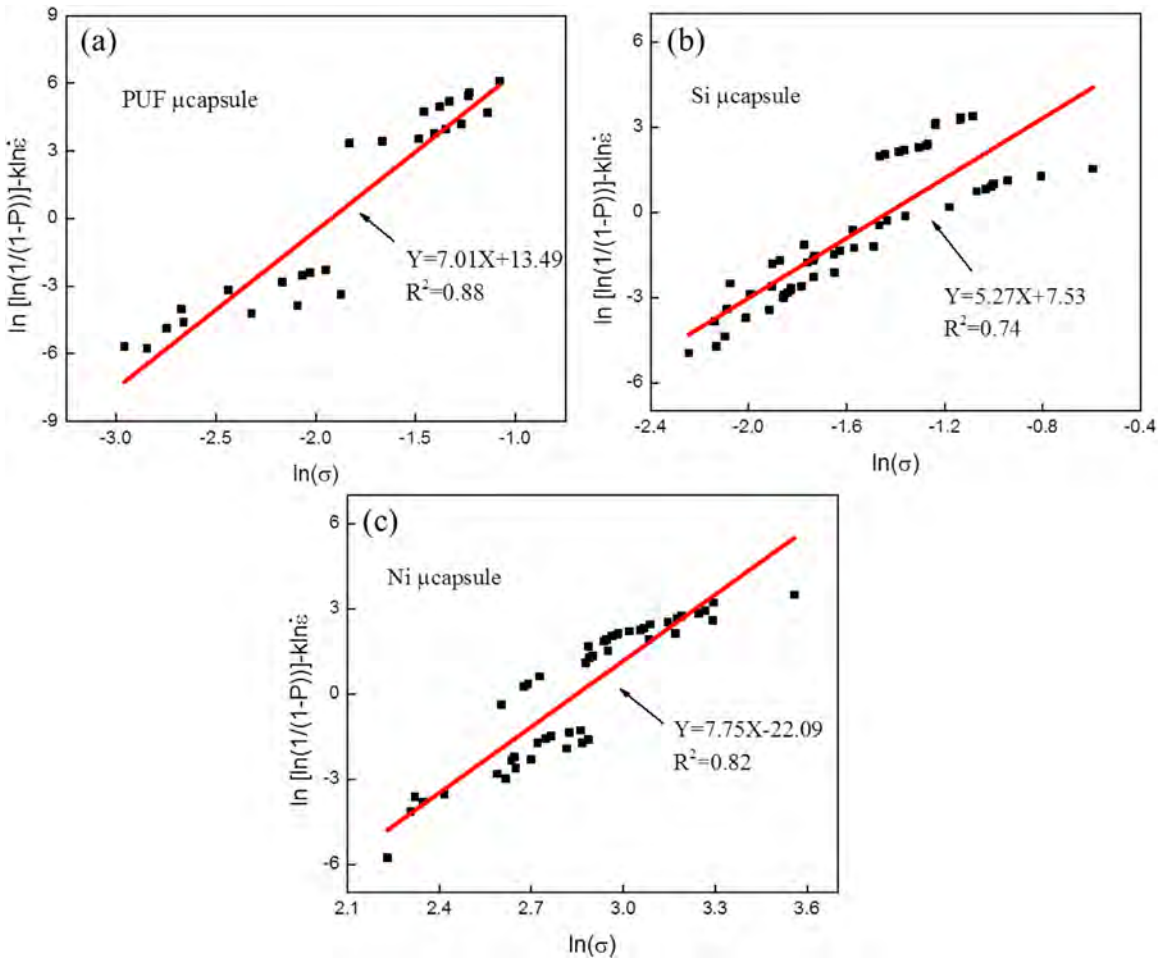

Fig. 11. Weibull distribution for the strength of (a) PUF, (b) Si, and (c) Ni microcapsules.

A linear relationship between $\ln\sigma$ and $\ln[\ln(1/(1-P_f))] - k\ln\dot{\varepsilon}$ can be derived from Eq. (18), as shown in Eq. (20).

$$\ln\left[\ln\left(\frac{1}{1-P_f(\sigma)}\right)\right] - k\ln\dot{\varepsilon} = m\ln\sigma - m\ln\sigma_{\dot{\varepsilon}} \tag{20}$$

Since the true value of $P_f(\sigma)$ is unknown, a prescribed estimator should be used. The cumulative probability of $P_f(\sigma)$ can be calculated from the experiment results using the following equation (Furnish et al., 2009; Sullivan and Lauzon, 1986),

$$P_f(\sigma_i) = \frac{i-0.5}{N} \tag{21}$$

where i represents the failure rank, σ_i represents the corresponding strength, and N represents the number of samples.

The value of k/m in Eq. (19) was obtained by curve fitting of data point obtained from experiments. The relationship of $\ln[ln(1/(1-P_f))] - kln\dot{\varepsilon}$ *versus* $\ln\sigma$ of different individual microcapsules can be found in Fig. 11. As can be seen, linear relationships can be observed for all three microcapsules. The slop indicates the Weibull modulus m. Given an initial k value, a new plot of linear relation can be drawn. After repeating process by adopting binary search strategy by using MATLAB software, m converges to a certain value which is the same value as calculated through Eq. (19).

It is known that larger m indicates smaller scattering in the strength of microcapsule (Sun et al., 2012). The m value for the Ni microcapsule is 7.75, which is larger than the other two microcapsules (7.01 for the PUF microcapsule and 5.27 for the Si microcapsule). This suggests that the Ni capsules are more homogenous. The Si microcapsule shows the lowest m value that may be attributed to the rough shell which may involve more defects, as shown in Fig. 7b2.

Mercade-Prieto et al. reported a m value of 2.22 for an oil-filled microcapsule with an average diameter of 17.6 μm (Mercade-Prieto et al., 2012). Huang et al. reported a m value of 3.37 for a glass sphere with a diameter about 4.4 mm (Huang et al., 2014). Wu et al. reported a m value of 4.1–5.3 for compressive strength of a spherical solid catalyst with a diameter around 5 mm (Wu et al., 2006). As can be seen, the Weibull moduli of the three microcapsules developed in the

Table 2
Statistics of the nominal strength of microcapsules under quasi-static loading.

Microcapsule types	Measured nominal strength		Nominal strength with fracture probability of 10% (MPa)
	Mean value (MPa)	Standard deviation (MPa)	
PUF	0.094	0.04	0.070
Silica	0.154	0.02	0.113
Nickel	13.983	3.13	11.017

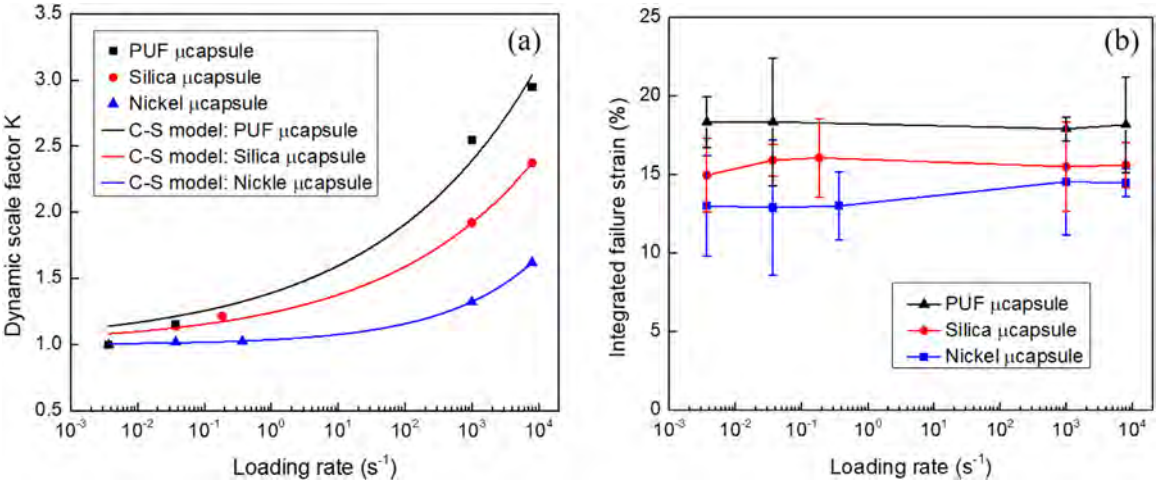

Fig. 12. (a) Dynamic scale factors and (b) integrated failure strains of microcapsules at different strain rates.

current study are higher than those reported in published literatures, suggesting good synthesis processes of microcapsules and reliable testing procedure. Moreover, the Weibull modulus is an empirical material constant which relates to the distribution of flaw size in the material. By using the inverse power law (Danzer, 1992), the relationship between the flaw size distribution factor (r_f) and the Weibull modulus can be described by the following equation,

$$r_f = \frac{m+2}{2} \tag{22}$$

It is known that larger r_f value represents smaller mean defect number per unit volume and defect size (Wu et al., 2007a). As can be seen from Eq. (22), the Weibull modulus is the only parameters related to the flaw size distribution factor. However, the Weibull modulus is affected by the shape and diameter of the microcapsule, flaws in the shell, measurement system, and many other factors. The obtained Weibull moduli of different microcapsules thus are helpful in understanding and optimization of the fabrication process and practical application of the microcapsules.

Table 2 summarizes the mean and standard deviation of measured nominal strength of the three microcapsules. Based on Weibull distribution assumption with the m value obtained from curve fitting, the nominal strength of microcapsule with fracture probability of 10% ($\sigma_{10\%}$) at quasi-static loading condition can be derived and summarized in Table 2. As can be seen, $\sigma_{10\%}$ of the Ni microcapsule is two orders higher than that of the PUF and the Si microcapsules, which reveals the robustness of Ni microcapsule for further application.

The dynamic scale factor K evaluates the rate dependence of microcapsules, which can be defined as the strength under corresponding loading rate divided by the strength at quasi-static loading rate (Brara and Klepaczko, 2006).

$$K = \frac{\sigma_c}{\sigma_q} \tag{23}$$

where σ_c is the strength of microcapsule under the corresponding loading rate, σ_q is the strength of the microcapsule at quasi-static loading. As can be seen from Fig. 12a, all the curves fit well with the C-S model with R square values larger than 0.97. The PUF microcapsule exhibits the largest dynamic scale factor followed by the Si microcapsule and the Ni microcapsule. This suggests the PUF microcapsule possesses the highest strain rate sensitivity. The integrated failure strain is also presented in Fig. 12b. For all the three microcapsules, the integrated failure strain remains relatively constant at different strain rates. Meanwhile, the PUF microcapsule shows the highest failure strain while the Ni microcapsule exhibits the lowest, which reveals that the PUF shell may have better ductility than the silica and the nickel shells.

Table 3
Parameters of C-S model for the three microcapsules.

Microcapsules	D	q	R^2
PUF	167	5.44	0.9718
Silica	1548	5.16	0.9919
Nickel	36,596	3.19	0.9996

Meanwhile, the dynamic scale factor K can be deduced from the Cowper-Symonds model (C-S model) as follows (Connolly et al., 2018; Kohar et al., 2016),

$$K = 1 + \left(\frac{\dot{\varepsilon}}{D}\right)^{1/q} \tag{24}$$

where $\dot{\varepsilon}$ is the strain rate, D and q are constants for specific material in the C-S model. The obtained material constants can be applied for further investigation including the development of analytic solution and FE simulation, which can regard the core-shell structure as one integral material (Wu and Thomson, 2007). Based on the parameters obtained from Table 3, it is convenient to predict the dynamic strength of fabricated microcapsules at different strain rates which is of great benefit to practical engineering applications.

4.2.3. Stiffness

In order to evaluate the stiffness of fabricated microcapsule, the Young's modulus can be investigated by using Hertz theory (Cordill et al., 2009; Gerberich et al., 2003). The contact force of sphere between two rigid flat plates can be expressed by the following equation.

$$F = \frac{4R^{1/2}}{3}\frac{E}{1-\nu^2}\left(\frac{d}{2}\right)^{3/2} \tag{25}$$

where F is the contact force, and R, E, ν, and d are the radius, the modulus, the Poison's ratio, and the deflection of microcapsule, respectively. Particularly, the reduced modulus of the microcapsules can be defined as follows,

$$E_r = E/\left(1-\nu^2\right) \tag{26}$$

The microcapsules can be assumed as a non-compressible material during compression (Chan et al., 2011), which is to say, the value of ν can be defined as 0.5. Based on the calculation, the modulus of the PUF, the Si, and the Ni microcapsules are 2.65 MPa, 3.52 MPa, and 500.25 MPa, respectively. As can be seen, the modulus of Ni microcapsule is two orders higher than the other two microcapsules.

4.2.4. Fracture mode

As described in theoretical model in Section 3.1, with the increase of the contact force and inner pressure, the third deformation stage may occur. The fracture modes of the three microcapsules under quasi-static compression are shown in Fig. 13a (PUF), Fig. 13b (Si), and Fig. 13c (Ni). Single crack (red arrow) from the top to the bottom contact surfaces was observed in all three microcapsules under quasi-static compression. Dynamic failure process was captured by the high speed camera with a time interval of 20 μs, as shown in Fig. 13d (PUF), Fig. 13e (Si), and Fig. 13f (Ni). Similar deformation was observed for three microcapsules as shown in Fig. 13d2, e2, and f2. However, a sharper angle of deformation can be found in the PUF microcapsule than that in the Si and the Ni microcapsules due to the lower stiffness of the PUF microcapsule, as indicated in the black dash rectangle in Fig. 13d3, e3, and f3. The liquid inside microcapsule can eject out (blue arrows) during the impact due to the high hydraulic pressure in the core material. The failure schematics based on Fig. 13d4, e4, and f4 are illustrated in Fig. 13d5 (PUF), Fig. 13e5 (Si), and Fig. 13f5 (Ni). It was observed that more cracks are generated in the three microcapsules under the dynamic impact. As can be seen, the Ni microcapsule may break into two main parts with several small debris and cracks (Fig. 13d6). The Si microcapsules may also fracture into several pieces (Fig. 13e6). However, the PUF microcapsule possesses a more localized failure (Fig. 13f6). Compared to the failure mode under quasi-static loading which only generates a single crack after failure, multiple cracks and fractures are often observed for microcapsules subjected to dynamic loading. That is because the crack may not have sufficient time to extend along the path of least resistance due to the rapidly increased stress at dynamic impact, which leads to localized fracture. The increased numbers of cracks may also help generate small debris to dissipate energy (Chen et al., 2013).

4.3. Mechanical properties of microcapsule-modified polymer

Typical compressive stress-strain curves of microcapsule-modified polymers under quasi-static loading are shown in Fig. 14a. As can be seen, the stress-strain curves possess three distinct stages. In the first stage, stress increases linearly with increasing stain up to 0.07 strain, followed by the second stage where the stress reduces slightly first with increasing strain up to 0.15 strain (Fig. 14b) and remains unchanged thereafter. Reduction in stress at the beginning of the second

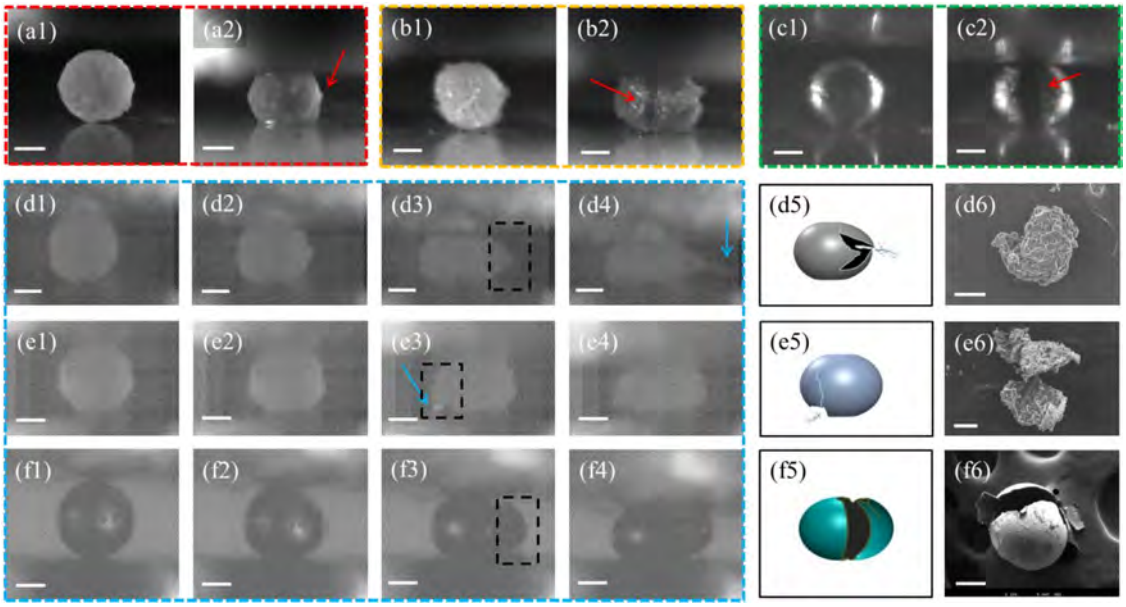

Fig. 13. Images of (a) PUF (b) Si, and (c) Ni microcapsules under quasi-static compression. Images of (d1–d4) PUF, (e1–e4) Si, and (f1–f4) Ni microcapsules under impact. Schematic drawing of failure morphology and FESEM images of (d5, d6) PUF, (e5, e6) Si, and (f5, f6) Ni microcapsules (Scale bars in the images represent 100 μm).

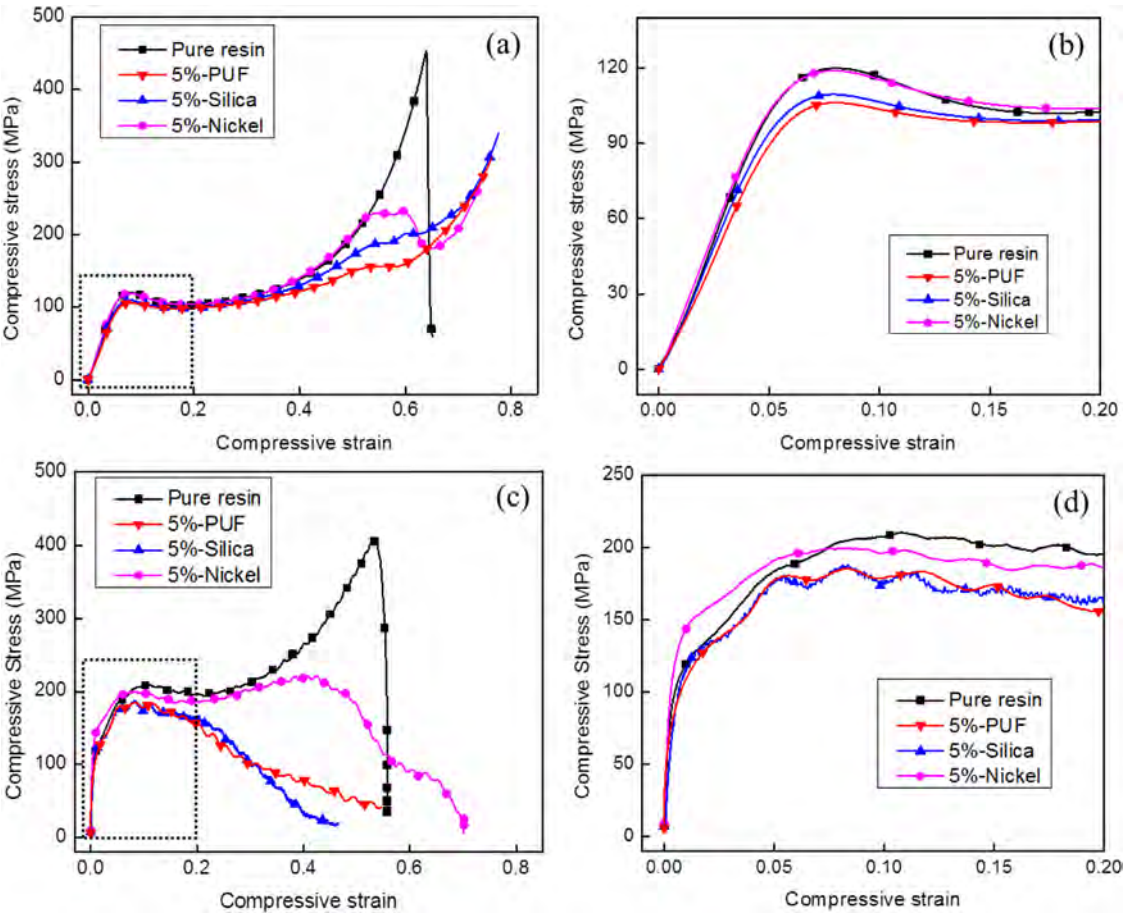

Fig. 14. Typical compressive stress *versus* compressive strain curves of microcapsule-modified epoxy resin at (a, b) quasi-static and (c, d) dynamic loadings.

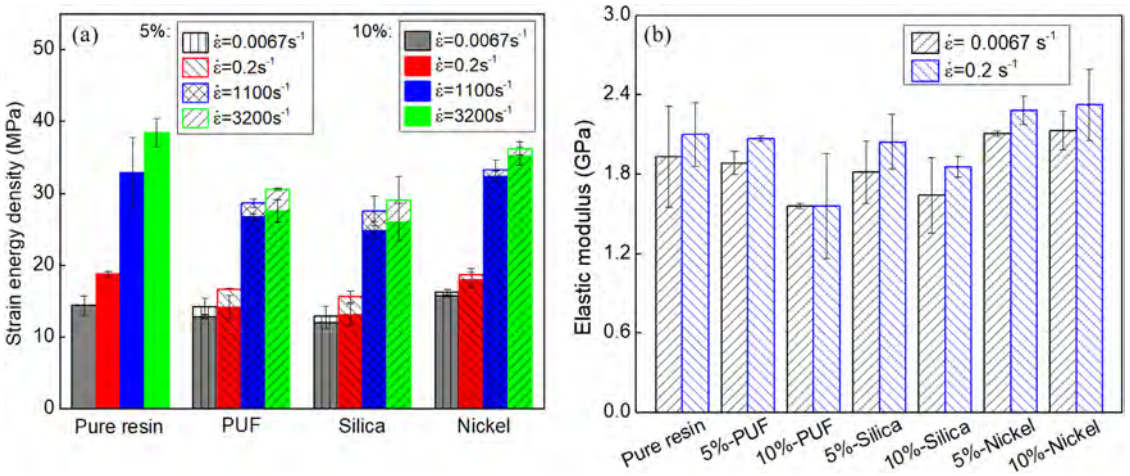

Fig. 15. (a) Strain energy absorption and (b) elastic moduli of microcapsule-modified epoxy resin.

stage may be attributed to stable crack propagation and fracture of microcapsule (Zhang et al., 2016). As can be seen from Fig. 14b, Ni microcapsule-modified polymer has comparable mechanical performance to the control group (*i.e.,* pure resin sample) and has much higher load capacity than the other two microcapsule-modified polymers in the first two stages. This is attributed to that the Ni microcapsule is much stronger than the PUF and the Si microcapsules. The third stage is the condensation stage where the specimen has been condensed and the stress rises up quickly till a catastrophic failure of the specimen, which is dominated by the combination of the mechanical property of the material and the structure property. As a result, only the first and second stages are investigated in this study.

Fig. 14c presents the stress-strain curves of microcapsule-modified polymers under dynamic loading. In general, the curves also possess three distinctive stages. However, reduction of stress at the beginning of the second stage under dynamic loading (Fig. 14d) is less pronounced than that under quasi-static loading. This may be attributed to more cracks are generated under impact loading to dissipate the impact energy. The increased crack propagation in the impact may smooth the strength loss than that of crack propagation in the quasi-static compression.

4.3.1. Energy absorption capacity

The strain energy density (U) of material can be evaluated by the following equation,

$$U = \int_0^{\varepsilon_s} \sigma(\varepsilon) d\varepsilon \tag{27}$$

where the upper bound of the integration interval ε_s is selected to be 0.2 strain for all loading conditions. This is to exclude the influence from the condensation stage and to ensure the calculated strain energy density can be used to compare the energy absorption capacity of different microcapsule-modified polymers (Fig. 15a). As can be seen, for all microcapsule-modified polymers, energy absorption capacity increases with increasing strain rate. The Ni microcapsule-modified polymer has comparable strain energy density to the pure resin at both quasi-static and dynamic compression, while both the PUF and the Si microcapsule-modified polymer show lower strain energy density because the PUF and the Si capsules are weaker than the Ni capsule. It is worth noting that the energy absorption capacity reduces with increasing microcapsule fraction. This is particularly true for the PUF and the Si microcapsule-modified polymers. This is because inclusion of the PUF and the Si microcapsules lowers the mechanical performance as well as the energy capacity of the resulting polymers. However, inclusion of the Ni microcapsules which are stronger and much robust, leads to less reduction in strain energy density of the resulting Ni microcapsule-modified polymer at higher capsule inclusion dosage.

4.3.2. Stiffness

The elastic modulus of specimen under quasi-static and higher strain rate compression can be found in Fig. 15b. As can be seen, for all microcapsule-modified polymers, the moduli increase with increasing strain rate. Compared to the control specimen (*i.e.,* pure resin), inclusion of the PUF or the Si microcapsules lowers the modulus of the resulting microcapsule-modified polymer and the moduli reduces with increasing microcapsule fraction. However, inclusion of the Ni capsules increases the modulus of the resulting microcapsule-modified polymer and the moduli increases with increasing microcapsule fraction. This suggests that the inclusion of microcapsule with high shell stiffness may enhance the stiffness of microcapsule-modified polymer.

Fig. 16a compares the elastic modulus of the microcapsule-modified polymers at different capsule fractions obtained from experiments and numerical simulations at static loading condition. As can be seen, the simulation results fit well with

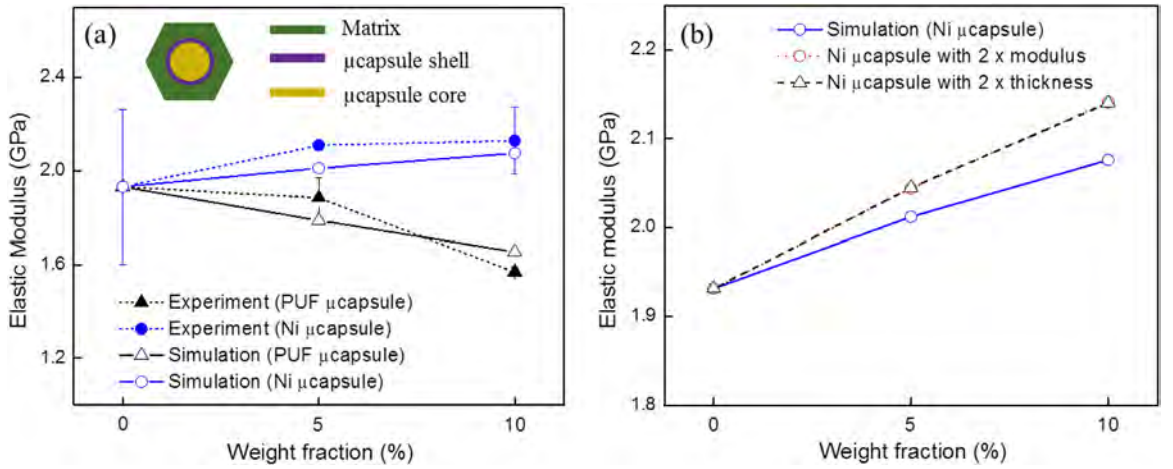

Fig. 16. (a) Elastic moduli of the PUF and the Ni microcapsule-modified polymers as a function of weight fraction (experiments *vs* simulations), and (b) effects of shell properties on the elastic moduli of the Ni microcapsule-modified polymer as a function of weight fraction (simulations).

the experiments for both the PUF and the Ni microcapsule-modified polymers. The elastic modulus of the Ni microcapsule-modified polymer increases while that of the PUF microcapsule-modified polymer decreases with increasing capsule dosage. Parametric studies were carried through numerical simulation to reveal the effects of shell properties on the elastic modulus of Ni microcapsule-modified polymer (Fig. 16b). As can be seen, the moduli improve dramatically when the shell thickness or the modulus of the shell material is doubled. The improvement is enlarged when the weight fraction of microcapsule increases. The results reveal that both the properties and the thickness of the shell play a key role in determining the elastic modulus of microcapsule-modified polymer.

4.3.3. Strength

The ratio of the strength increase of microcapsule-modified polymer to strength of the pure resin (η_σ) can be calculated from the following equation,

$$\eta_\sigma = \frac{\sigma_e - \sigma_p}{\sigma_p} \times 100\% \tag{28}$$

where σ_e is the strength of microcapsule-modified polymer at a specific strain rate, which is defined as the maximum stress of the polymer at the first stage, and σ_p is the strength of pure resin at the same strain rate. The values of η_σ for microcapsule specimens can be found in Fig. 17. An approximate 5% increase can be observed for nickel microcapsule with both 5% and 10% weight fraction. However, the value of η_σ will decrease after strain rate 0.2 and the decrease values are less than 5% which remains relatively constant. As a result, the importation of Ni microcapsule may not influence the strength of epoxy resin significantly. For both PUF and Si microcapsule specimens, the strength will decrease dramatically as high as 25%. Moreover, decrease trends can be observed for them with the increase of strain rate, which indicate that the addition of PUF or Si microcapsule will decrease the strength of matrix resin and its strain rate sensitivity.

Fig. 18 plots the compressive strengths of pure resin and microcapsule-modified polymers with different weight fractions at different strain rates. As can be seen, the strength of Ni microcapsule shows close value with the strength of pure resin no matter the weight fraction of the microcapsule and the strain rate. PUF microcapsule and Si microcapsule behave relatively close compressive strength which is much lower than that of pure resin and Ni microcapsule. The compressive strength of all four polymers increases linearly with increasing strain rate in logarithm scale. Thus, the strength may be expressed as a function of the strain rate as follows,

$$\sigma = m \cdot log\dot{\varepsilon} + A \tag{29}$$

where σ is the strength of polymer, $\dot{\varepsilon}$ is the strain rate, A is a material constant, and m can be regarded as the strain rate sensitivity index. Through curve fitting, corresponding parameters of linear models for the four polymers are summarized in Table 4. A very good correlation was achieved for all the fittings as all the residual squares are larger than 0.98.

The pure resin samples show largest strain rate sensitivity index which is attributed to that the strain rate dependency of the polymer is significantly determined by the strain rate sensitivity of the matrix material (Balch et al., 2005). Ni microcapsule-modified polymer is more sensitive than the other two microcapsule-modified polymers. This can be explained as more energy can be dissipated in the Ni microcapsule-modified polymer than the other two microcapsule-modified polymers due to the higher strength of the Ni microcapsule. The better energy dissipation capacity may lead to higher strain rate sensitivity (Li et al., 2009). However, the different strain rate sensitivity indexes of the PUF and Si microcapsule-modified polymers also suggest that the filled microcapsule play an important role in determining the strain rate sensitivity of the microcapsule-modified polymer (Gupta and Shunmugasamy, 2011).

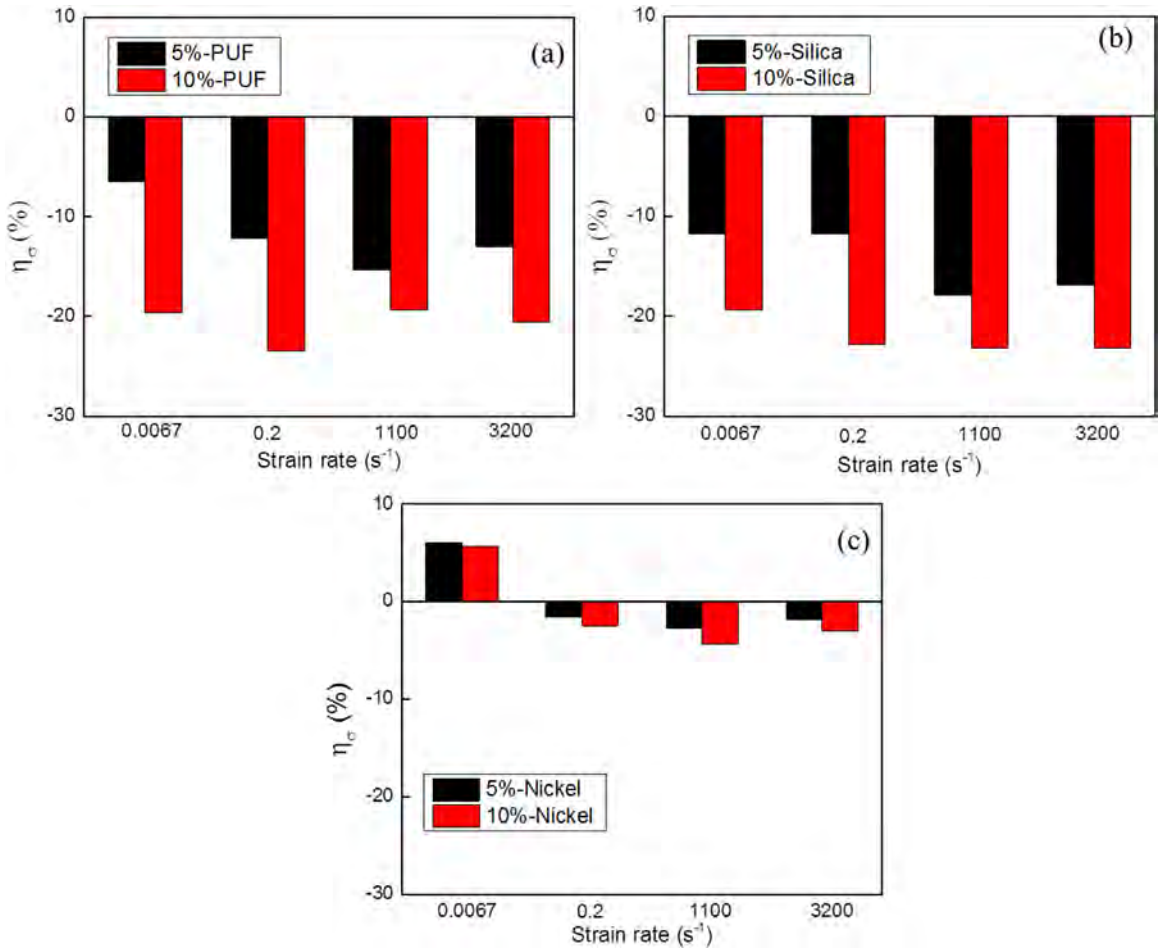

Fig. 17. η_σ of (a) PUF, (b) Si, and (c) Ni microcapsule-modified polymers.

Table 4
Parameters used for the linear model of microcapsule-modified epoxy resin.

Parameters	Pure resin	PUF		Silica		Nickel	
		5%	10%	5%	10%	5%	10%
m	20.20	16.31	16.39	15.54	14.99	18.65	18.19
A	137.84	121.87	109.11	121.19	107.36	137.94	136.55
R^2	0.9973	0.9847	0.9898	0.9969	0.9932	0.9873	0.9856

The strength of polymer modified with 5 wt.% PUF (or Ni) microcapsules at high strain rate loading (3300 s^{-1}) were studied through FE analysis (Fig. 18). As can be seen, the strengths resulted from FE analysis are very close to those obtained from experiments, which prove the validity of the FE model. Similarly, the strength of the microcapsule-modified polymers at the medium strain rates (20–200 s^{-1}) can be obtained numerically, which is often difficult to obtain experimentally. This is again of great importance for the design and optimization of the microcapsule-modified polymers.

5. Discussions

5.1. Fracture of microcapsule at different loading conditions

The fracture mechanism of Ni microcapsule under two rigid plate compression (Fig. 19a) and Ni microcapsule-modified polymer under compression (Fig. 19b) is studied and compared. As can be seen, for individual capsule under compression (Fig. 19a), the stress is concentrated in the contact area where the microcapsule is in contact with the two rigid plates. Cracks initiate at the two contact areas and propagate along the meridional direction, which is similar to the description in Section 3.2.4. For capsule embedded in polymer matrix (Fig. 19b), the stress is distributed on the entire surface of the

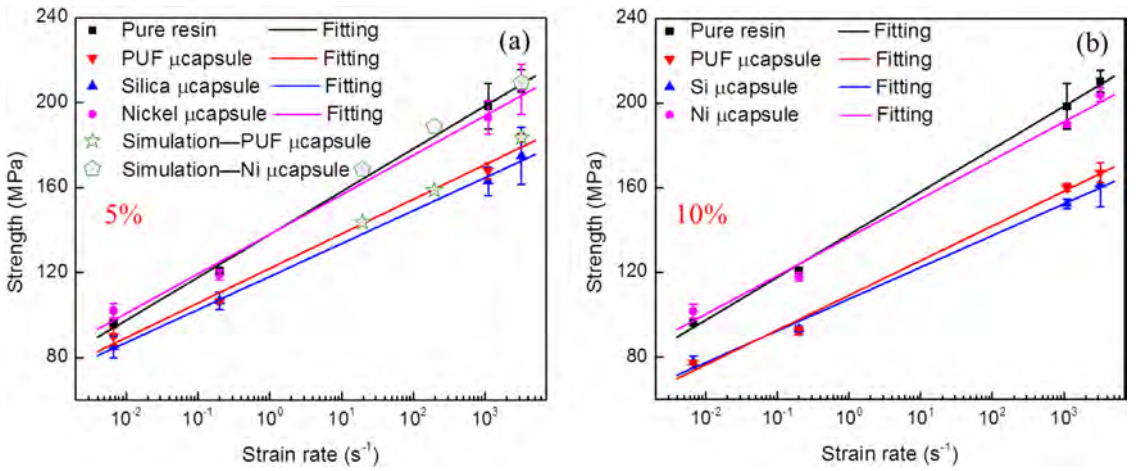

Fig. 18. Compressive strength of microcapsule-modified epoxy resin with (a) 5% and (b) 10% microcapsules at different strain rates (log).

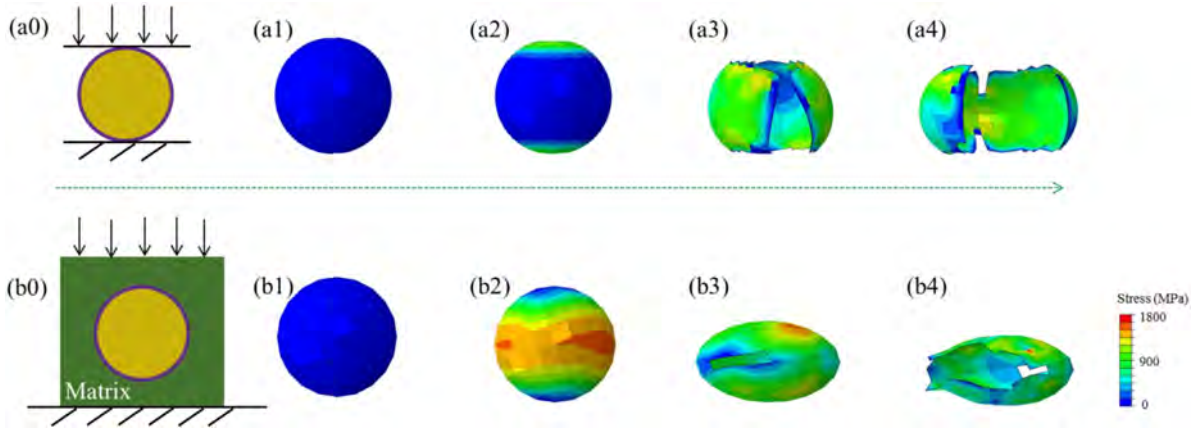

Fig. 19. The fracture mode of (a) Ni microcapsule under two rigid plate compression and (b) Ni microcapsule-modified polymer under compression.

microcapsule but higher stress level is observed on the annular equatorial area which leads to final crack propagation along the equatorial direction. Due to a more uniform stress distribution on the entire capsule, a higher mechanical performance can be expected for microcapsules embedded in matrix.

5.2. Fracture modes of microcapsule-modified polymer

5.2.1. Experimental observation

The fracture surface of three different microcapsule modified epoxy resin can be found in Fig. 20. Fig. 20a1 shows the OM images of the fracture surface of nickel shell microcapsule modified epoxy resin. All the PUF shell microcapsules at the fracture surface have been broken since only part of the shell has been left. Fig. 20a2 and a3 illustrate that some of the cracks pass through the PUF shell microcapsule and break them into pieces, as indicated by the dash lines and red arrows. This phenomenon can be explained as during the impact test, the crack propagates to the microcapsule and passes through the microcapsule due to the lower strength of PUF shell microcapsule than that of the matrix material. Similar morphology was observed in the fracture surface of the Si shell microcapsule-modified polymer. Cracks pass through microcapsules and fracture of microcapsules with multiple breakages can be observed in Fig. 20b2 and b3. Both the PUF and the Si shell microcapsules show good interfacial bond with epoxy resin since the microcapsules bond well with the matrix even after fracture, as indicated in Fig. 20a4 and b4. The fractured Ni microcapsules remain spherical shape which indicates that the Ni microcapsules provide resistance to sliding of surround polymer matrix even after their breakages due to their higher strength. This phenomenon may also increase the energy absorption capacity which has been shown in Fig. 15a. Fig. 20c2 and c3 show distinct partial breakage of the nickel shell microcapsules as indicated by red arrows. However, intact Ni microcapsules were also observed as indicated by the blue arrow. This can be explained by the critical debonding stress theory discussed in Section 3.2. As can be seen, smaller microcapsule requires higher critical stress to cause debonding. Meanwhile, smaller microcapsule may also possess higher nominal strength than the larger capsule. As a result, it will be

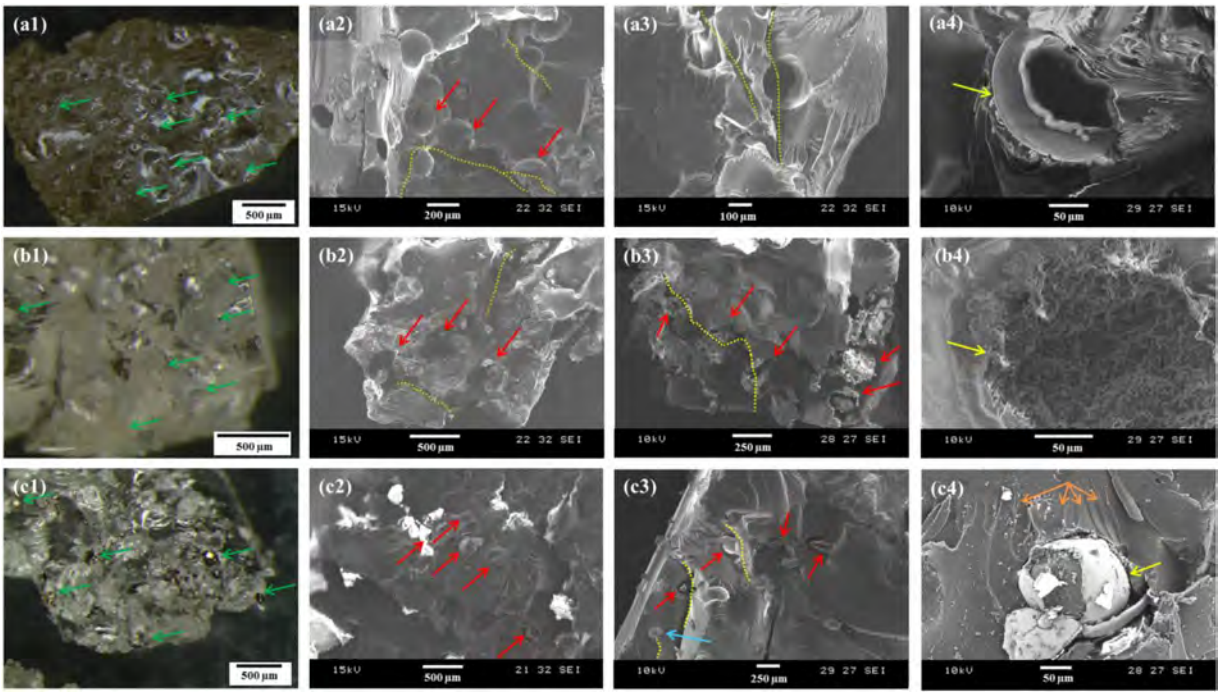

Fig. 20. Fracture surfaces of (a) PUF, (b) Si, and (c) Ni microcapsule-modified epoxy resin after dynamic loading.

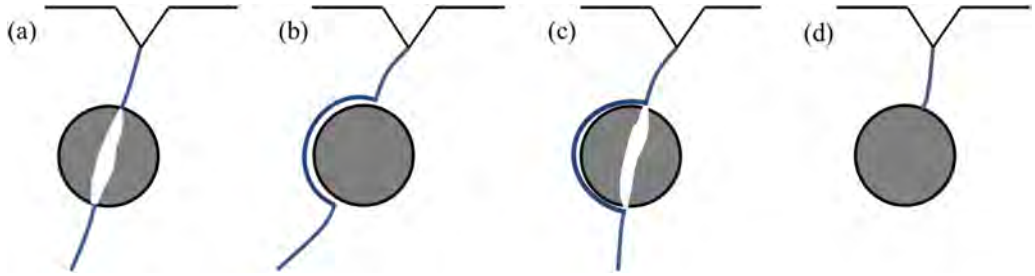

Fig. 21. Schematic illustration of failure modes in microcapsule-modified polymer.

more difficult for the cracks to debond and pass through the smaller microcapsules due to the higher critical stress and higher strength of the microcapsule, which may cause crack pining, as shown in Fig. 20c3.

Potential failure modes of microcapsule-modified polymer are depicted in Fig. 21. As can be seen, for weak microcapsules such as the PUF or the Si microcapsules, crack tends to penetrate through the capsule directly (Fig. 21a). For microcapsules with weak interfacial bond in a weak matrix, crack tends to propagate along the capsule/matrix interface as shown in Fig. 21b. After debonding; however, large plastic deformation of the surrounding matrix may lead to sliding of fracture surfaces which leads to fracture of the microcapsule as illustrated in Fig. 21c. This represents the failure mode observed in the Ni microcapsule-modified polymer (Fig. 20c). Strong capsule/matrix interfacial bond was also observed in Ni microcapsule-modified polymer as crack tails (Jin et al., 2011) can be found on the fracture surface as indicated in Fig. 20c4 (orange arrows). The superior capsule/matrix interfacial bond and robust mechanical properties of the Ni microcapsule can potentially lead to crack pinning as shown in Fig. 21d and toughening of the resulting modified polymer.

5.2.2. Finite element analysis

The fracture mode of the PUF microcapsule-modified polymer can be found in Fig. 22. Fig. 22a shows the von Mises stress distribution in the epoxy matrix. As can be seen, stress distribution in the matrix is not uniform. Stress concentrates on the interface between the microcapsule and the matrix and connects in between adjacent microcapsules. The area of concentrated stress increases with increasing compressive strain. Localized cracks occur as indicated by the red arrows and the cracks propagate as indicated by the black arrow. Further compression leads to cracks connection (circulated in black dash line) and failure of the matrix. The stresses are released after the failure of matrix. The failure progress of the PUF microcapsules is presented in Fig. 22b. As can be seen, the stress concentrates at the equator area of the microcapsules. With the increase of compressive strain, cracks form at the equator area as indicated by the black arrows. All microcapsules

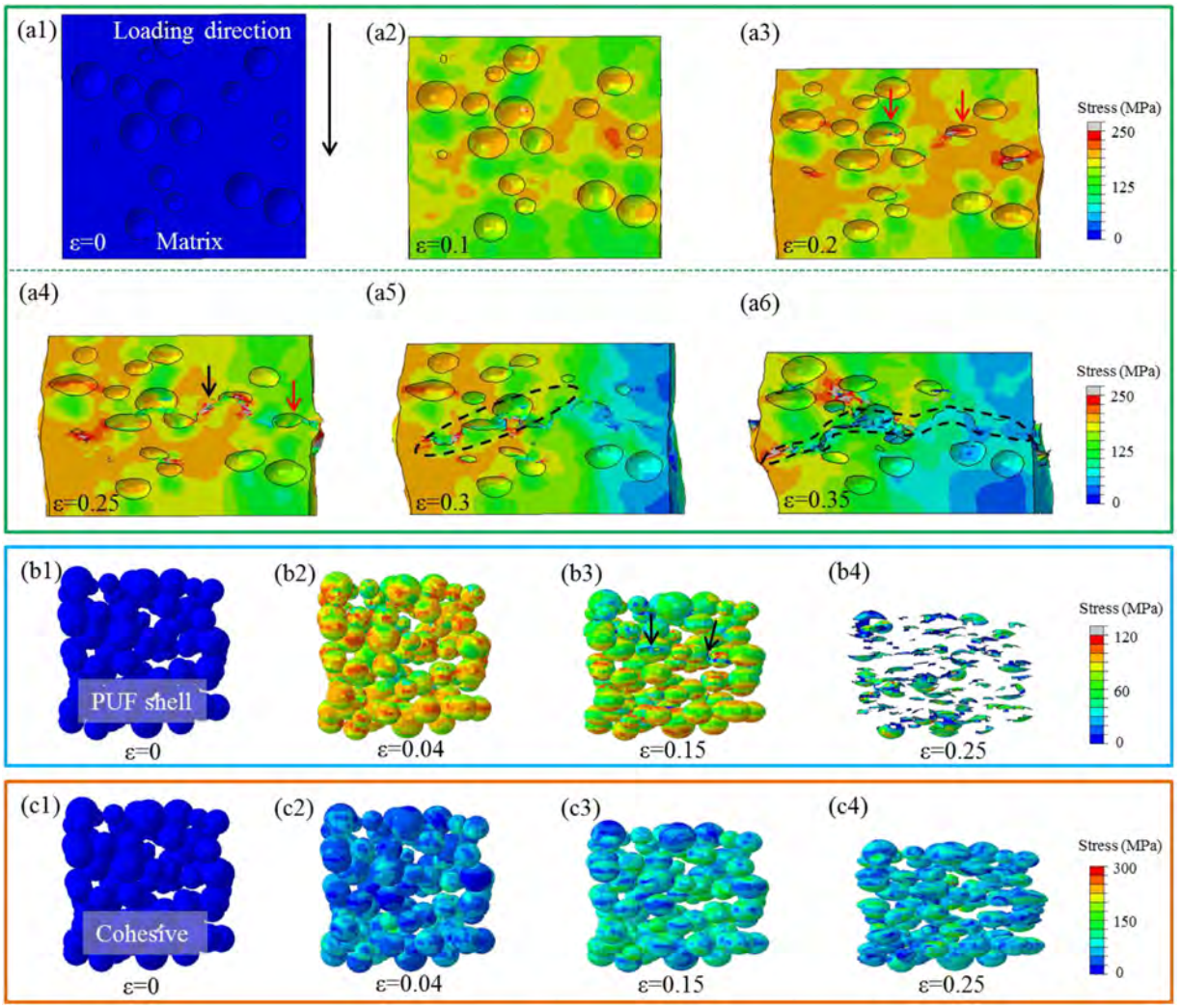

Fig. 22. The von Mises stress distribution in (a) the epoxy matrix, (b) the PUF microcapsules, and (c) the cohesive layer between PUF microcapsule and epoxy matrix.

are fractured at a compressive strain of about 0.25. However, the cohesive elements remain intact without damage during the compression, which reveals that the PUF microcapsules are fractured without debonding from the matrix during the compression as described in Fig. 21.

The fracture mode of the Ni microcapsule-modified polymer can be found in Fig. 23. Fig. 23a plots the von Mises stress distribution in the epoxy matrix. As can be seen, the stress concentrates at the interface between the microcapsules and the matrix, which may lead to local cracks (red arrow) in the epoxy resin. After that, the localized cracks converge to large cracks (black arrow) which lead to local damages (black dash line) in the matrix. The damages connect with each other which result in fracture of the specimen. The stress distribution in the Ni microcapsules is shown in Fig. 23b. Again, the stress concentrates at the equator area of the microcapsules and the microcapsules are fractured at a compressive strain of about 0.4. The cohesive elements, however, fail before the fracture of the Ni microcapsule as shown in Fig. 23c. This confirms the failure mode of Ni microcapsule-modified polymer as described in Fig. 21c.

5.3. Effect of shell thickness on performance of Ni microcapsule-modified polymer

It is known from Section 3.2.1 that the shell thickness increase can improve the nominal strength of the individual microcapsule. It is of great interest to investigate the mechanical property of microcapsule-modified polymer with stronger microcapsule. Fig. 23d compares the stress distribution of the Ni microcapsules with thicker shell (2 × and 4 ×) in the Ni microcapsule-modified polymers. As can be seen, no obvious fracture can be observed for Ni microcapsules with four times

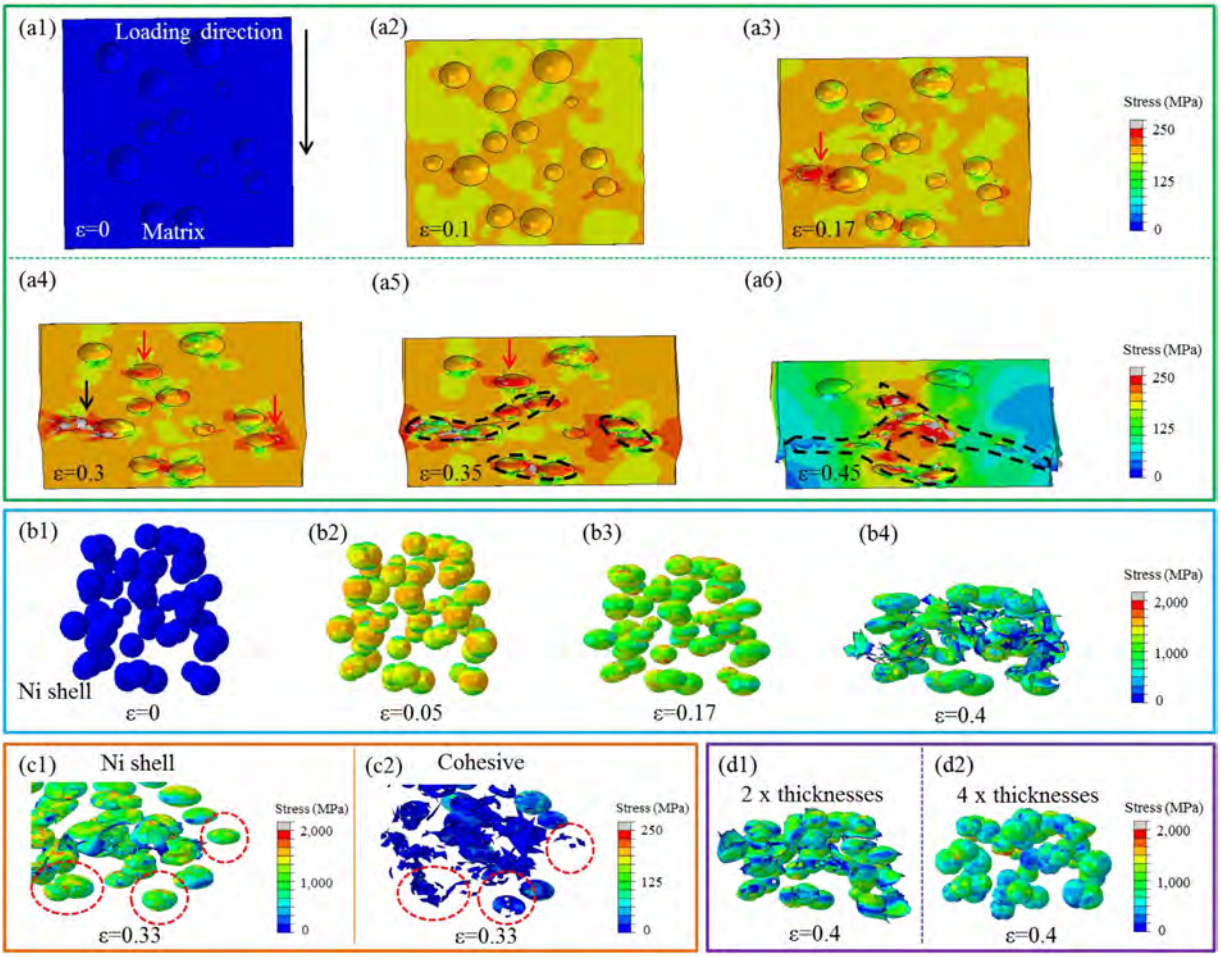

Fig. 23. The von Mises stress distribution in (a) the epoxy matrix, (b) the Ni microcapsules, (c) the Ni microcapsules and the cohesive layers between the Ni microcapsules and the epoxy matrix, and (d) Ni microcapsules with increased shell thickness.

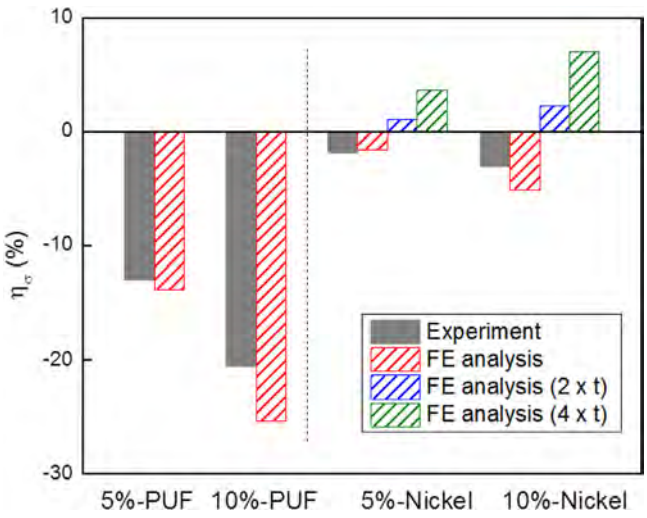

Fig. 24. η_σ of PUF and Ni microcapsule-modified polymers.

shell thickness. It indicates that the microcapsule may not fracture during the compression when the microcapsules are very strong, which may hinder the intended functions (*e.g.,* self-healing) of the microcapsules.

The ratio of the strength increase (η_σ) of materials at strain rate of 3300 s^{-1} at both experiment and FE analysis is also studied, as shown in Fig. 24. The results from the experiment and the FE analysis fit well with each other in both PUF and Ni microcapsule-modified polymer at different weight fraction, which prove the validity of the FE simulation. A dramatic increase trend can be found with the increased shell thickness which reveals that the shell thickness influences the mechanical properties of microcapsule-modified polymer significantly. It can be observed that when the shell thickness of the Ni microcapsule is two times or larger than the original thickness, the strength of the microcapsule-modified polymer can be improved. As a result, the introduction of nickel shell may not significantly reduce or even increase the load bearing capability of epoxy resin while the introduction of silica and PUF shell microcapsules may decrease the strength of the matrix material significantly. The superior performance of Ni microcapsule is of great importance to impart both strength and functionality into the resulting microcapsule-modified polymers.

6. Conclusions

This study investigates the mechanical performance of individual microcapsule with different shell types (PUF, Si, and Ni) and corresponding microcapsule-modified polymers under quasi-static compression as well as dynamic impact. Finite element modeling is carried out to investigate the strength and the failure mechanism of both the individual microcapsule and the microcapsule-modified epoxy resin. Results indicate that the strength of Ni microcapsule is much more robust than the PUF and the Si microcapsules at different strain rates. All three types of microcapsules show significant strain rate effects, which can be described by the C-S model. More cracks and fragments are observed in microcapsule subject to dynamic loading, which indicates higher energy dissipation under impact.

Ni microcapsule-modified epoxy resin shows comparable strength to the pure epoxy resin at different strain rates, while both PUF and Si microcapsule-modified epoxy resins exhibit significant reduction in their strengths. All microcapsule-modified epoxy resins possess a linearity relationship between the compressive strength and the strain rate. However, Ni microcapsule-modified polymer shows high strain rate sensitivity in compressive strength than the other two microcapsule-modified polymers. Ni microcapsule-modified polymer shows distinct failure modes when compared to the PUF and the Si microcapsule-modified polymers. As the PUF and the Si microcapsules are weak, matrix cracks penetrate through the microcapsules which results in the final failure. Thus, catastrophic failure of PUF and Si microcapsule are observed at the fracture surfaces of microcapsule-modified polymers. The Ni microcapsule, on the other hand, is much stronger, and thus matrix cracks tend to propagate along the microcapsule/epoxy matrix interface, which results in debonding between the microcapsules and the epoxy matrix. After debonding, sliding of the fracture surfaces may lead to fracture of some weaker Ni microcapsules.

Declaration of Competing Interests

The authors declare that they have no known competing financial interests or personal relationships that could have appeared to influence the work reported in this paper.

CRediT authorship contribution statement

Xin Zhang: Conceptualization, Investigation, Writing - original draft. **Pengfei Wang:** Methodology, Writing - review & editing. **Dawei Sun:** Data curation, Formal analysis. **Xin Li:** Data curation, Software. **Jinliang An:** Data curation, Formal analysis. **T.X. Yu:** Formal analysis, Methodology, Supervision. **En-Hua Yang:** Formal analysis, Methodology, Supervision, Writing - review & editing. **Jinglei Yang:** Conceptualization, Formal analysis, Supervision, Writing - review & editing.

Acknowledgments

The authors would like to acknowledge the DRTech-DIRP grant, NSFC/RGC Joint Research Scheme of Hong Kong (Grant#: N_HKUST 631/18), and Zhongshan-HKUST Program (Project ID: RG066) to support this research. Sincere thanks are given to Dr. He Zhang, Dr. Fei Shen, and Dr. Yongbing Chong for their constructive suggestions and supports on this work.

References

Balch, D.K., O'Dwyer, J.G., Davis, G.R., Cady, C.M., Gray, G.T., Dunand, D.C., 2005. Plasticity and damage in aluminum syntactic foams deformed under dynamic and quasi-static conditions. Mat. Sci. Eng. A-Struct. 391, 408–417.

Bao, R.H., Yu, T.X., 2015. Collision and rebound of ping pong balls on a rigid target. Mater Des. 87, 278–286.

Brara, A., Klepaczko, J., 2006. Experimental characterization of concrete in dynamic tension. Mech. Mater. 38, 253–267.

Brown, E.N., Sottos, N.R., White, S.R., 2002. Fracture testing of a self-healing polymer composite. Exp. Mech. 42, 372–379.

Chan, E.-S., Lim, T.-K., Voo, W.-P., Pogaku, R., Tey, B.T., Zhang, Z., 2011. Effect of formulation of alginate beads on their mechanical behavior and stiffness. Particuology 9, 228–234.

Chen, X.D., Wu, S.X., Zhou, J.K., 2013. Experimental and modeling study of dynamic mechanical properties of cement paste, mortar and concrete. Constr. Build Mater 47, 419–430.

Connolly, D.S., Kohar, C.P., Mishra, R.K., Inal, K., 2018. A new coupled thermomechanical framework for modeling formability in transformation induced plasticity steels. Int. J. Plast. 103, 39–66.
Cordill, M.J., Moody, N.R., Gerberich, W.W., 2009. The role of dislocation walls for nanoindentation to shallow depths. Int. J. Plast. 25, 281–301.
Cross, R., 2014. Impact behavior of hollow balls. Am. J. Phys. 82, 189–195.
Danzer, R., 1992. A general strength distribution function for brittle materials. J. Eur. Ceram Soc. 10, 461–472.
Dilsiz, N., Wightman, J.P., 2000. Effect of acid-base properties of unsized and sized carbon fibers on fiber/epoxy matrix adhesion. Colloid Surface A 164, 325–336.
Do, T., Ko, Y.G., Jung, Y., Choi, U.S., 2020. Highly durable and thermal-conductive shell-coated phase change capsule as a thermal energy battery. ACS Appl. Mater Interf.
Furnish, M.D., Chhabildas, L.C., Reinhart, W.D., Trott, W.M., Vogler, T.J., 2009. Determination and interpretation of statistics of spatially resolved waveforms in spalled tantalum from 7 to 13 GPa. Int. J. Plast. 25, 587–602.
Gent, A.N., 1980. Detachment of an elastic matrix from a rigid spherical inclusion. J. Mater Sci. 15, 2884–2888.
Gerberich, W.W., Mook, W.M., Perrey, C.R., Carter, C.B., Baskes, M.I., Mukherjee, R., Gidwani, A., Heberlein, J., McMurry, P.H., Girshick, S.L., 2003. Superhard silicon nanospheres. J. Mech. Phys. Solids 51, 979–992.
Guo, Y., Ruan, Q., Zhu, S., Wei, Q., Lu, J., Hu, B., Wu, X., Chen, H., Fang, D., Li, Y., 2019. Dynamic failure of titanium: temperature rise and adiabatic shear band formation. J. Mech. Phys. Solids.
Gupta, N., Nagorny, R., 2006. Tensile properties of glass microballoon-epoxy resin syntactic foams. J. Appl. Polym. Sci. 102, 1254–1261.
Gupta, N., Shunmugasamy, V.C., 2011. High strain rate compressive response of syntactic foams: trends in mechanical properties and failure mechanisms. Mat. Sci. Eng. A-Struct. 528, 7596–7605.
Huang, J., Xu, S., Yi, H., Hu, S., 2014. Size effect on the compression breakage strengths of glass particles. Powder Technol. 268, 86–94.
Huang, R.X., Li, P.F., Liu, T., 2016. X-ray microtomography and finite element modelling of compressive failure mechanism in cenosphere epoxy syntactic foams. Compos Struct. 140, 157–165.
Jin, H., Miller, G.M., Sottos, N.R., White, S.R., 2011. Fracture and fatigue response of a self-healing epoxy adhesive. Polymer (Guildf) 52, 1628–1634.
Keller, M.W., Sottos, N.R., 2006. Mechanical properties of microcapsules used in a self-healing polymer. Exp. Mech. 46, 725–733.
Kim, K., Cheng, J., Liu, Q., Wu, X.Y., Sun, Y., 2010. Investigation of mechanical properties of soft hydrogel microcapsules in relation to protein delivery using a mems force sensor. J. Biomed. Mater. Res. Part A 92A, 103–113.
Kohar, C.P., Cherkaoui, M., El Kadiri, H., Inal, K., 2016. Numerical modeling of trip steel in axial crashworthiness. Int. J. Plast. 84, 224–254.
Li, P., Petrinic, N., Siviour, C.R., 2012. Finite element modelling of the mechanism of deformation and failure in metallic thin-walled hollow spheres under dynamic compression. Mech. Mater. 54, 43–54.
Li, P., Petrinic, N., Siviour, C.R., Froud, R., Reed, J.M., 2009. Strain rate dependent compressive properties of glass microballoon epoxy syntactic foams. Mat. Sci. Eng. A-Struct. 515, 19–25.
Li, V.C., Herbert, E., 2012. Robust self-healing concrete for sustainable infrastructure. J. Adv. Concr. Technol. 10, 207–218.
Li, W.T., Zhu, X.J., Zhao, N., Jiang, Z.W., 2016. Preparation and properties of melamine urea-formaldehyde microcapsules for self-healing of cementitious materials. Materials (Basel) 9.
Marur, P.R., 2004. Estimation of effective elastic properties and interface stress concentrations in particulate composites by unit cell methods. Acta Mater 52, 1263–1270.
Mercade-Prieto, R., Allen, R., York, D., Preece, J.A., Goodwin, T.E., Zhang, Z., 2012. Determination of the failure stresses for fluid-filled microcapsules that rupture near the elastic regime. Exp. Mech. 52, 1435–1445.
Nguyen, N.Q., Gupta, N., 2010. Analyzing the effect of fiber reinforcement on properties of syntactic foams. Mat. Sci. Eng. A-Struct. 527, 6422–6428.
Ni, M.Z., Li, M., Mao, D.L., 2012. Adhesion improvement of epoxy molding compound - Pd Preplated leadframe interface using shaped nickel layers. Microelectron. Reliab. 52, 206–211.
O'Sullivan, M., Zhang, Z., Vincent, B., 2009. Silica-shell/oil-core microcapsules with controlled shell thickness and their breakage stress. Langmuir 25, 7962–7966.
Patrick, J.F., Robb, M.J., Sottos, N.R., Moore, J.S., White, S.R., 2016. Polymers with autonomous life-cycle control. Nature 540, 363–370.
Pauchard, L., Rica, S., 1998. Contact and compression of elastic spherical shells: the physics of a 'Ping-Pong' ball. Philosoph. Mag. B-Phys. Condensed Matter Stat. Mech. Electron. Opt. Mag. Propert. 78, 225–233.
Pejchal, V., Zagar, G., Charvet, R., Denereaz, C., Mortensen, A., 2017. Compression testing spherical particles for strength: theory of the meridian crack test and implementation for microscopic fused quartz. J. Mech. Phys. Solids 99, 70–92.
Prak, D.J.L., Lee, B.G., Cowart, J.S., Trulove, P.C., 2017. Density, viscosity, speed of sound, bulk modulus, surface tension, and flash point of binary mixtures of butylbenzene plus linear alkanes (n-Decane, n-Dodecane, n-Tetradecane, n-Hexadecane, or n-Heptadecane) at 0.1 MPa. J. Chem. Eng. Data 62, 169–187.
Reissner, E., 1949. On the theory of thin elastic shells. B Am. Math. Soc. 55, 295 -295.
Rule, J.D., Sottos, N.R., White, S.R., 2007. Effect of microcapsule size on the performance of self-healing polymers. Polymer (Guildf) 48, 3520–3529.
Sarı, A., Alkan, C., Karaipekli, A., 2010. Preparation, characterization and thermal properties of PMMA/n-heptadecane microcapsules as novel solid–liquid microPCM for thermal energy storage. Appl. Energy 87, 1529–1534.
Shipway, P.H., Hutchings, I.M., 1993. Attrition of brittle spheres by fracture under compression and impact loading. Powder Technol. 76, 23–30.
Sullivan, J., Lauzon, P., 1986. Experimental probability estimators for weibull plots. J. Mater. Sci. Lett. 5, 1245–1247.
Sun, D., Zhang, H., Zhang, X., Yang, J., 2019. Robust metallic microcapsules: a direct path to new multifunctional materials. ACS Appl. Mater. Interfaces 11, 9621–9628.
Sun, G.Z., Pang, J.H.L., Zhou, J.Y., Zhang, Y.N., Zhan, Z.Y., Zheng, L.X., 2012. A modified weibull model for tensile strength distribution of carbon nanotube fibers with strain rate and size effects. Appl. Phys. Lett. 101.
Swetha, C., Kumar, R., 2011. Quasi-static uni-axial compression behaviour of hollow glass microspheres/epoxy based syntactic foams. Mater Design 32, 4152–4163.
Vandegaer, J.E., 2012. Microencapsulation: Processes and Applications. Springer Science & Business Media.
Vu, C.C., Weiss, J., Ple, O., Amitrano, D., Vandembroucq, D., 2018. Revisiting statistical size effects on compressive failure of heterogeneous materials, with a special focus on concrete. J. Mech. Phys. Solids 121, 47–70.
Wang, P., Yang, J., Sun, G., Zhang, X., Zhang, H., Zheng, Y., Xu, S., 2018. Twist induced plasticity and failure mechanism of helical carbon nanotube fibers under different strain rates. Int. J. Plast.
Wang, P.F., Zhang, X., Hansen, R.V., Sun, G.Z., Zhang, H., Zheng, L.X., Yu, T.X., Lu, G.X., Yang, J.L., 2016. Strengthening and failure mechanisms of individual carbon nanotube fibers under dynamic tensile loading. Carbon NY 102, 18–31.
White, S.R., Sottos, N.R., Geubelle, P.H., Moore, J.S., Kessler, M.R., Sriram, S.R., Brown, E.N., Viswanathan, S., 2001. Autonomic healing of polymer composites. Nature 409, 794–797.
Wu, D.F., Zhou, J.C., Li, Y.D., 2006. Distribution of the mechanical strength of solid catalysts. Chem. Eng. Res. Des. 84, 1152–1157.
Wu, D.F., Zhou, J.C., Li, Y.D., 2007a. Mechanical strength of solid catalysts: recent developments and future prospects. Aiche J. 53, 2618–2629.
Wu, G., An, J., Sun, D., Tang, X., Xiang, Y., Yang, J., 2014. Robust microcapsules with polyurea/silica hybrid shell for one-part self-healing anticorrosion coatings. J. Mater. Chem. A 2, 11614–11620.
Wu, G.C., Yang, J.M., Hahn, H.T., 2007b. The impact properties and damage tolerance and of bi-directionally reinforced fiber metal laminates. J. Mater Sci. 42, 948–957.
Wu, W.J., Thomson, R., 2007. A study of the interaction between a guardrail post and soil during quasi-static and dynamic loading. Int. J. Impact Eng. 34, 883–898.

Xue, S.L., Li, B., Feng, X.Q., Gao, H.J., 2016. Biochemomechanical poroelastic theory of avascular tumor growth. J. Mech. Phys. Solids 94, 409–432.
Yaghoubi, A.S., Liaw, B., 2013. Effect of lay-up orientation on ballistic impact behaviors of glare 5 FML beams. Int. J. Impact Eng. 54, 138–148.
Yang, J.L., Keller, M.W., Moore, J.S., White, S.R., Sottos, N.R., 2008. Microencapsulation of isocyanates for self-healing polymers. Macromolecules 41, 9650–9655.
Yin, T., Rong, M.Z., Zhang, M.Q., Yang, G.C., 2007. Self-healing epoxy composites - Preparation and effect of the healant consisting of microencapsulated epoxy and latent curing agent. Compos Sci. Technol. 67, 201–212.
Yu, M., Zhu, P., Ma, Y.Q., 2012. Experimental study and numerical prediction of tensile strength properties and failure modes of hollow spheres filled syntactic foams. Comp. Mater Sci. 63, 232–243.
Yuan, J.L., Zhao, X.W., Ye, L., 2015. Structure and properties of urea-formaldehyde resin/polyurethane blend prepared via in-situ polymerization. Rsc. Adv. 5, 53700–53707.
Yuan, Y.C., Rong, M.Z., Zhang, M.Q., Chen, J., Yang, G.C., Li, X.M., 2008. Self-healing polymeric materials using epoxy/mercaptan as the healant. Macromolecules 41, 5197–5202.
Zhang, L.J., D'Acunzi, M., Kappl, M., Imhof, A., van Blaaderen, A., Butt, H.J., Graf, R., Vollmer, D., 2010. Tuning the mechanical properties of silica microcapsules. Phys. Chem. Chem. Phys. 12, 15392–15398.
Zhang, X., Wang, P.F., Sun, D.W., Li, X., Yu, T.X., Yang, E.H., Yang, J.L., 2018. Rate dependent behaviors of nickel-based microcapsules. Appl. Phys. Lett. 112.
Zhang, X., Wang, P.F., Zhou, Y.H., Li, X.T., Yang, E.H., Yu, T.X., Yang, J.L., 2016. The effect of strain rate and filler volume fraction on the mechanical properties of hollow glass microsphere modified polymer. Compos Part B-Eng. 101, 53–63.